Haptic Augmentation for Teleoperation through Virtual Grasping Points

Michael Panzirsch, Ribin Balachandran, Bernhard Weber, Manuel Ferre, Jordi Artigas

Abstract—Future challenges in teleoperation arise from a new complexity of tasks and from constraints in unstructured environments. In industrial applications as nuclear research facilities, the operator has to manipulate large objects whereas medical robotics requires extremely high precision. In the last decades, research optimized the transparency in teleoperation setups through accurate hardware, higher sampling rates and improved sensor technologies. To further enhance the performance in telemanipulation, the idea of haptic augmentation has been briefly introduced in [Panzirsch et al., IEEE ICRA, 2015, pp. 312317]. Haptic augmentation provides supportive haptic cues to the operator that promise to ease the task execution and increase the control accuracy. Therefore, an additional haptic interface can be added into the control loop. The present paper introduces the stability analysis of the resulting multilateral framework and equations for multi-DoF coupling and time delay control. Furthermore, a detailed analysis via experiments and a user study is presented. The control structure is designed in the network representation and based on passive modules. Through this passivity-based modular design, a high adaptability to new tasks and setups is achieved. The results of the user study indicate that the bimanual control brings large benefits especially in improving rotational precision.

Index Terms—haptic augmentation, multilateral teleoperation, MPMT, TDPA.

1 Introduction

One of the most sophisticated technologies developed for telepresence is telemanipulation that allows separating individuals from the environment they manipulate, ideally without even noticing. Therefore, a robot with manipulation capabilities and a haptic interface are needed to allow a user to teleoperate the robot and reproduce the sense of touch to the user based on the physical interaction between the robot and the manipulated object. The bilateral controller is a central element of any telemanipulation system since it is responsible for conveying the commands of the human operator from the haptic interface to the robot and vice-versa. These commands describe current motions and forces of both, human and robot. Bilateral control has long attracted the attention of control engineers due to the special closed-loop characteristics established by the communication channel between robot and operator.

To increase manipulation capabilities by additional slave robots [1], [2] or for training applications in a Mentor−Novice training setup [3], [4] , research shifted on to multilateral control in the recent past. More general, multilateral control allows controlling n robots through m different haptic interfaces, where usually but not necessarily, $m \geq n$ [5], [6], [7]. Based on this method, in [8], the concept of haptic augmentation has been introduced in a Dual-Master-Single-Slave setup. Analogous to visually augmented telepresence, using haptic augmentation, additional information can be provided through the teleoperator's haptic channel which has the potential of enhancing the operator's feeling of immersion in the remote environment, easing the task execution e.g. through guidance or higher manipulation dexterity.

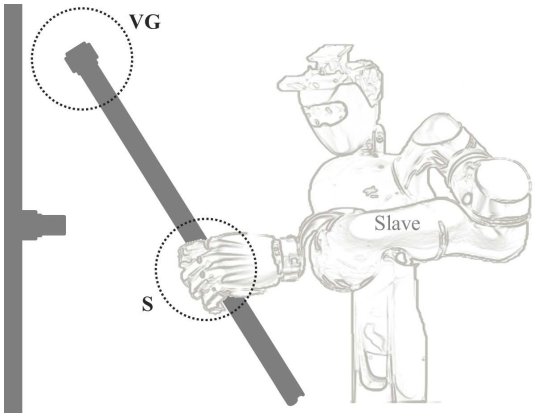

Fig. 1. Slave Robot Grasping Pipe

In this paper, the haptic augmentation focuses on the improvement of precision in the rotatory degrees of freedom (DoF). Since the assembly of large structures with bulky objects requires a high level of dexterity, because translational and rotational movements need to be properly combined, a pipe handling scenario is presented. Especially, the manipulation of large objects requires aids since the point of interaction with the environment may be distant from the grasping position on the object. For instance, placing a long pipe in a hole requires high precision in rotatory motions at one pipe end while maintaining the position (close to the hole) of the other end of the pipe. Rotating one end of a long object may cause unwanted translations at the other end. Comparable to a baseball racket, the orientation of large devices can be more easily set via two points of interaction. Similarly, the manipulation can be haptically augmented by providing the operator with control and

- *Michael Panzirsch, Ribin Balachandran, and Jordi Artigas are with the department for Analysis and Control of Advanced Robotic Systems, German Aerospace Center, Oberpfaffenhofen, Germany.*
- *Bernhard Weber is with the department for Perception and Cognition, German Aerospace Center, Oberpfaffenhofen, Germany.*
- *Michael Panzirsch and Prof. Manuel Ferre are with the Universidad Politécnica de Madrid, Centre for Automation and Robotics (CAR) UPM-CSIC, Madrid, Spain.*
  E-mail: michael.panzirsch@dlr.de

*Manuscript received *Month *Day, *Year; revised *Month *Day, *Year.*

This article has been accepted for publication in a future issue of this journal, but has not been fully edited. Content may change prior to final publication. Citation information: DOI 10.1109/TOH.2018.2809746, IEEE Transactions on Haptics

force feedback information on a second interaction point through a second input device. In [8], this concept has been realized with only one slave robot and two master devices as depicted in Fig. 1 and Fig. 2. Via a multilateral coupling, the master M1 controls the robot hand S directly while the master M2 controls a virtual grasping point VG as the point of interaction with the environment. In this framework, a Cartesian task allocation can be implemented that assigns the dominance of one master device in a desired point of interaction. Besides the manipulation of large

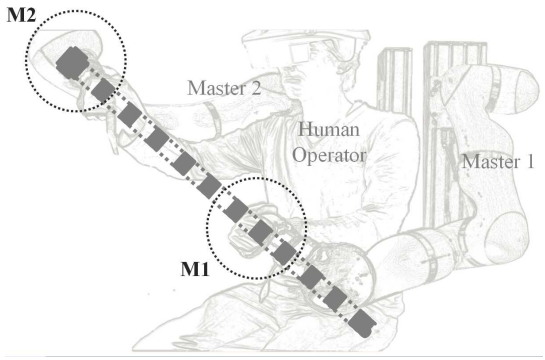

Fig. 2. Operator with Two Masters and Virtual Pipe

objects, e.g. the manipulation of medical probes as ultrasonic devices that need to be applied with especially high accuracy is demanding with one hand or telemanipulator respectively. A second hand helps to set the orientation, to maintain a contact force and to compensate disturbances that can result e.g. from the patient's body or connected cables. Other tasks requiring high rotational accuracy without environment interaction are the measurement of temperature and distance, welding etc.. Note that this concept is reasonable for teleoperation and haptic interaction in virtual realities as well since it can be implemented in the control algorithms of the master devices.

In literature, different approaches have been presented to provide additional assistance to the operator and that are comparable with the haptic augmentation concept. The authors of [9] proposed a haptic intention augmentation concept for cooperative telemanipulation that has been tested in a space setup. In [10], the end-effector of a kinematically redundant slave manipulator is controlled by one of the masters whereas the null space motion is controlled by another, without influencing the end-effector pose of the slave. An adaptive control is applied in [11] to introduce projective force mappings which impose specific boundaries on the slave robot's motion. In [12], two master devices with different degrees of freedom control a slave device with three DoFs wherein the haptic feedback could be displayed only on the available DoFs of the master devices. The concept of disjoint axis control was introduced in [13] to distribute the control of the two subsets of the available DoFs of a redundant slave robot (mobile platform with a serial manipulator). Similar setups have been proposed in [14] and [15]. In the bimanual telerobotic surgery setup of [16], the reaction force of an action induced by one hand was haptically augmented to the other hand to avoid instability issues. These works provide control interfaces that are more powerful than simple bilateral controllers. Still, the concept of haptic augmentation involving the virtual grasping point method as well as the Cartesian task allocation considered here was so far only presented in [8].

This paper is premised on the work in [8] which introduced the basic concept and a rough evaluation through experiments. First of all, the coupling implementation in separate DoFs in [8] is replaced by a multi-DoF implementation using spatial springs. In addition, novel haptic augmentation principles are introduced that promise to increase the coupling rigidity and prevent constrained robot configurations. Also, concepts are proposed that serve the online adaption of the grasping point position and increase intuitiveness so that the command of rotations via counteracting forces is enabled. A more prevalent time delay control approach than in [8] is applied and besides more detailed experiments, the haptic augmentation is evaluated with a user study. For increased experimental control and in order to underline the applicability of haptic augmentation in virtual realities (VR), the user study is performed in a VR environment. To emphasize the generality of the proposed virtual grasping point approach, besides this Dual-Master-Single-Slave setup, an application of the concept to cooperatively grasping slaves with kinematic coupling is briefly presented in the appendix of this manuscript.

The main contributions of this paper are:

- The multi-DoF implementation considering spatial springs
- An interface for online variation of the virtual grasping point's position with respect to the slave robot
- A controller extension that allows the command of rotations through counteracting forces
- The enhancement of the task allocation in the Cartesian space to achieve a more rigid coupling and for prevention of constrained robot configurations
- Implementation of the Time Domain Passivity Approach [17] in a multi-DoF setup with position-position architecture
- An objective evaluation based on a user study
- The application of the virtual grasping point concept to cooperatively grasping slave robots

The paper is structured as follows: In Section 2, the fundamental technologies are presented. The multi-DoF implementation of the virtual grasping point method is presented and its stability is evaluated in Section 3. The task allocation and the related contributions are explained in Section 4. Furthermore, its passive behavior will be discussed. The passivity control of the delayed communication channel is presented in Section 5. Experiments and a user study will be presented in Section 6 and Section 7 respectively. Section 8 summarizes the results to a conclusion.

2 FUNDAMENTALS

In this chapter, the basic control principles relevant for haptic augmentation will be explained. First, the bilateral control scheme for teleoperation and the applied stability principle are introduced. Later, this setup is extended to the multilateral case.

2.1 Bilateral Track Design

In a general bilateral teleoperation system, a human operator (HO) can command the motion of a robot (slave) in its environment through his/her input device (master). A common method to achieve this is to couple the slave robot electronically to the motion of the master device through a PI controller. The proportional P-part of the controller acts on the velocity error of both devices similar to a damping element and the integrative I-part, on the position error of both devices like a spring. Fig. 3 shows the signal flow diagram of a Position-Position (PP, [18]) scheme, which includes time delays in both directions, T_1 and T_2. In this

This article has been accepted for publication in a future issue of this journal, but has not been fully edited. Content may change prior to final publication. Citation information: DOI 10.1109/TOH.2018.2809746, IEEE Transactions on Haptics

configuration, position or velocity signals (delayed velocity $v_{3/9}^{del}$) are exchanged and the feedback forces $F_{3/9}$ result from a pair of PI-controllers.

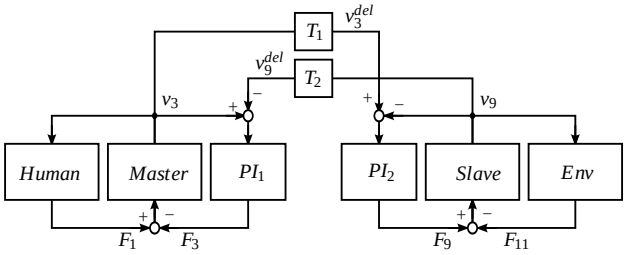

Fig. 3. Signal Flow Diagram of a Teleoperation System with Position-Position Architecture

2.2 Stability Concept

To guarantee the stability of a bilateral system without time delay, e.g. the frequency-based Routh-Hurwitz (stability of LTI systems), Raisbeck (passivity) or Llewellyn (absolute stability) criteria can be used. In order to handle the destabilizing effect of time delay, methodologies like wave variable transformations, time domain passivity approach (TDPA) or the two-layer approach [19] can be applied. Those approaches rely on the passivity of a system with states **x**:

$$V(\mathbf{x}(t)) - V(\mathbf{x}(0)) \leq \int_0^t s(\mathbf{u}(\tau),\mathbf{y}(\tau))d\tau = \int_0^t \mathbf{y}^T(\tau)\mathbf{u}(\tau)d\tau. \quad (1)$$

As long as the energy increase in the system since $t = 0$, $V(\mathbf{x}(t)) - V(\mathbf{x}(0))$ is not higher than the integral of the power (supply rate s, input **u** and output **y**) that has entered the system, the system hasn't generated energy itself. In other words, the system is passive and thus $\mathscr{L}_2$-stability can be guaranteed [20], [21].

2.2.1 Network Representation

The energy behavior of a system can be systematically analyzed by the so-called network representation. To derive the network representation of the signal-flow-diagram of Fig. 3, its subsystems need to be transduced into their electrical analogues (Fig. 4). The Methodology for Passivity-based Multilateral Teleoperation (MPMT, [7]) provides two main modules for bilateral teleoperation networks: agents and tracks. An agent can be a human operator with its master device or the slave in its environment.The track represents the software part of the teleoperator containing controllers and the time delay power network (TDPN) that has been introduced in [22], [23]. The TDPNs guarantee the power consistency of transmitted signals in the communication channel. The electrical analogues of the proportional and the integrative parts of the PI-controllers are resistance and capacitance respectively. The set of PI controllers of track Γi will be hereafter referred to as $PI_{\Gamma i}$. The mechanical models of human operator and the environment consist of mass, spring and damper which are analogous to inductance, capacitance and resistance respectively in the electrical domain. The master and slave devices are modeled as mass-damper or inductance-resistance systems. The teleoperation system is split up into two directions of energy flow:

- R2L: the communication from right to left, which is represented by the upper part of the track in Fig. 4 including $TDPN_1$ and PI_1. The velocity source v_9 represents the power input from the *Agent* $\Lambda 2$ side.
- L2R: the communication from left to right, which is represented by the lower part of the track in Fig. 4 including $TDPN_2$ and PI_2. The velocity source v_3 represents the power input from the *Agent* $\Lambda 1$ side.

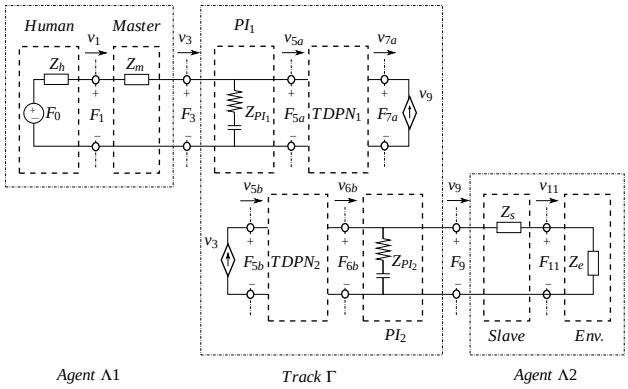

Fig. 4. Network Representation of a Position-Position Architecture with MPMT Modules Track and Agent

In [24], it was shown that networks consisting of passive subsystems are also passive and therefore $\mathscr{L}_2$-stable. The agents can be assumed to be passive as they behave passively in their interaction. A human operator dissipates the energy that has been introduced by the environment and vice-versa. Therefore, the $\mathscr{L}_2$-stability of a bilateral system can be guaranteed if the track subsystem is designed in a passive manner.

2.2.2 Energy Observation

In the network representation, the energy behavior of a 2-port (see Fig. 5) can easily be analyzed. $E_{P1/P2}$ are the energies on port $P1$

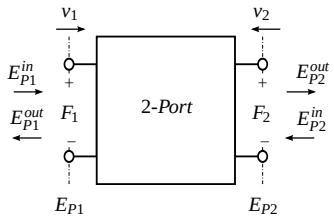

Fig. 5. In and Out Energies of a 2-port Network

or port $P2$ of a 2-port. To guarantee passivity the following has to hold:

$$E_{P1}(t) + E_{P2}(t) \geq 0. \quad (2)$$

The power $P_{P1/P2}$ can be computed based on conjugate power pairs (force and velocity) at each port:

$$P_{P1/P2}(t) = v_{1/2}(t)F_{1/2}(t) \quad (3)$$

For instance, in the case of a delay in the 2-port, the energies on left and right side cannot be calculated at the same time.

This article has been accepted for publication in a future issue of this journal, but has not been fully edited. Content may change prior to final publication. Citation information: DOI 10.1109/TOH.2018.2809746, IEEE Transactions on Haptics

Therefore, the power has to be split up considering the flow directions ($P^{in/out}_{P1/P2}$) via the sign of $P_{P1/P2}$:

$$P^{in}_{P1}(t) = \begin{cases} 0, & \text{if } P_{P1}(t) < 0 \\ P_{P1}(t), & \text{if } P_{P1}(t) > 0 \end{cases} \quad \text{and} \tag{4}$$

$$P^{out}_{P1}(t) = \begin{cases} 0, & \text{if } P_{P1}(t) > 0 \\ -P_{P1}(t), & \text{if } P_{P1}(t) < 0. \end{cases} \tag{5}$$

The subindices *in* and *out* indicate the power (or energy) flowing *into* and *out* of the network on the left or the right side respectively. The in/out flowing energies $E^{in/out}_{P1/P2}$ on the left/right side of the 2-port can be computed through integration over time:

$$E^{in/out}_{P1/P2}(t) = \int_0^t P^{in/out}_{P1/P2}(\tau)\, d\tau. \tag{6}$$

2.3 Multilateral Structure

The aim of a multilateral teleoperation system is the haptic coupling of multiple devices with the aid of control software. The design of a multilateral system becomes very generic with the MPMT since different types of modules can be assembled. Therefore, the system can be easily adapted for new tasks and setups. Fig. 6 depicts a trilateral system consisting of two types of agents, three tracks and three power control units (PCU). Those PCU subsystems are MPMT modules that manage the power distribution between one agent and the connected tracks. Since the PCU [7] and Agents are passive, additionally, only the tracks need to be designed in a passive manner to guarantee the overall passivity of the multilateral system.

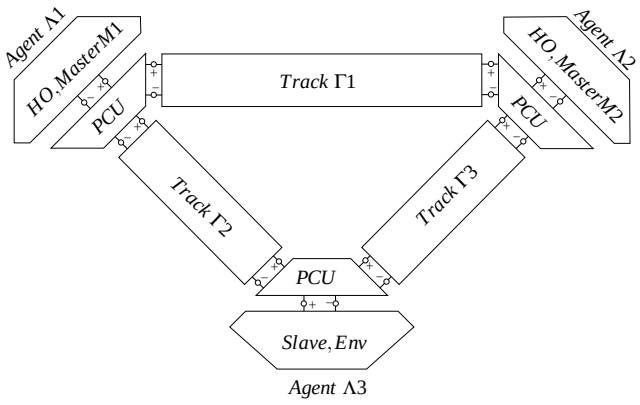

Fig. 6. Network Representation of a Trilateral Teleoperation System with PCU [7]

3 Virtual Grasping Point

As mentioned before, a pipe handling scenario is presented that represents several aspects of the large field of applications for haptic augmentation concepts. A system with a bimanual input device and a slave robot arm grasping a large pipe (compare Fig. 1 and Fig. 2) is considered.

Fig. 7 depicts the pipe kinematic-based coupling of the three devices master M1, master M2 and slave S. The tool center points (TCP) of the three devices with respect to the world frame are depicted with the frames ${}^{W}H_{M1/M2/S}$. Note that the grasping frame ${}^{W}H_{G}$ in which the slave hand grasps the pipe, is defined by the pipe axis and differs from the slave frame ${}^{W}H_{S}$. The vector g in ${}^{W}H_{S}$ and the distance $d+a$ determines the pipe end ${}^{W}H_{VG}$ in which the virtual grasping point is defined. The VG position ${}^{W}H_{VG}$ (vector g and distance d) can be set e.g. automatically through stereo vision. For the sake of simplicity the VG was not matched automatically for the experiments later presented. Though the virtual grasping point can be chosen arbitrarily in the slave's environment, the pipe end is the optimal location for the focused task. Through an additional input device as a pair of buttons, the scalar a, the distance of the virtual grasping point VG from the grasping point G, can be varied online. This is reasonable in certain tasks like manipulation of an ultrasonic device with virtual grasping points, since the rotational accuracy increases with the distance but also larger motions of the master M2 are necessary. Therefore, the distance should be adaptable. The desired position ${}^{W}H^{des}_{VG}$ of the VG with respect to master M2 is referred to the initial real VG position ${}^{W}H_{VG}$. Analogously, the desired position ${}^{W}H^{des}_{G}$ of the grasping point G with respect to master M1 is referred to the initial real grasping point position ${}^{W}H_{G}$. ${}^{W}H_{\tilde{VG}}$ is the VG position with respect to master M1. The spatial spring A couples master M1 and slave S in the grasping point and spatial springs B and C couple master M2 and slave S and master M1 and master M2 respectively in the virtual grasping point VG. The nomenclature is summarized in Table 1.

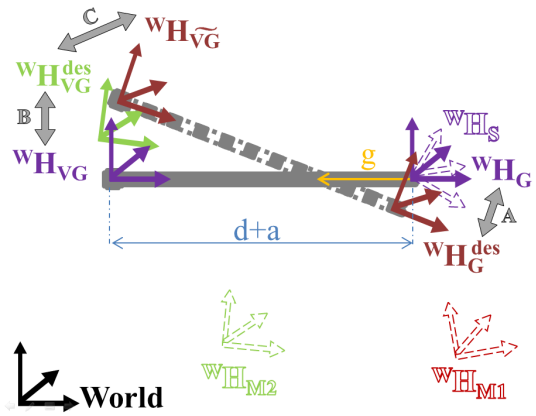

Fig. 7. Real and Virtual Pipe with Coordinate Frames

TABLE 1
Nomenclature

Γ1	Track coupling master M1 and master M2
Γ2	Track coupling master M1 and slave S
Γ3	Track coupling master M2 and slave S
${}^{W}H_{S}$	Tool center point of slave S
${}^{W}H_{M1}$	Tool center point of master M1
${}^{W}H_{M2}$	Tool center point of master M2
${}^{W}H_{G}$	Grasping point in tool center point of slave S
${}^{W}H_{VG}$	Virtual grasping point w.r.t. ${}^{W}H_{G}$
${}^{W}H^{des}_{G}$	Grasping point w.r.t. master M1
${}^{W}H_{\tilde{VG}}$	Virtual grasping point w.r.t. ${}^{W}H^{des}_{G}$
${}^{W}H^{des}_{VG}$	Virtual grasping point in tool center point of master M2

3.1 Implementation

Here, the multi-DoF implementation of the virtual grasping point method is presented. The orientation of the slave ${}^{W}R_{S}$ has to be projected onto their connecting axis through the rotation matrix R_{Pr} into the grasping frame ${}^{W}R_{G}$:

$$ {}^{W}R_{G} = {}^{W}R_{S}R_{Pr} \tag{7} $$

with

$$ R_{Pr} = \left[\begin{array}{ccc} \frac{r_1}{\|r_1\|_2}, & \frac{r_2}{\|r_2\|_2}, & \frac{r_3}{\|r_3\|_2} \end{array} \right] \quad \text{and} \tag{8} $$

$$ r_1 = g, \tag{9} $$

$$ r_2 = \left[\begin{array}{c} 0 \\ -r_{1,3} \\ r_{1,2} \end{array} \right], \tag{10} $$

$$ r_3 = r_1 \times r_2. \tag{11} $$

The pose ${}^{W}H_{VG}$ of the virtual grasping point VG can be calculated with the distance $d+a$ as follows

$$ {}^{W}H_{VG} = \left[\begin{array}{cc} {}^{W}R_{G} & {}^{W}p_{S} + {}^{W}R_{G}de_1 + {}^{W}R_{G}ae_1 \\ 0 & 1 \end{array} \right], \quad \text{with} \tag{12} $$

$$ e_1 = [1\ 0\ 0]^T. \tag{13} $$

${}^{W}p_{S}$ is the position of the slave device and ${}^{W}p_{M1/M2}$ are the positions of left and right masters respectively. The desired positions of the grasping ${}^{W}p_{G}^{des}$ and virtual grasping point ${}^{W}p_{VG}^{des}$ are

$$ {}^{W}p_{G}^{des} = {}^{W}p_{S}^{t_0} + {}^{W}p_{M1} - {}^{W}p_{M1}^{t_0}, \tag{14} $$

$$ {}^{W}p_{VG}^{des} = {}^{W}p_{VG}^{t_0} + {}^{W}p_{M2} - {}^{W}p_{M2}^{t_0}. \tag{15} $$

With ${}^{W}R_{VG}^{t_0} = {}^{W}R_{G}^{t_0}$ and

$$ {}^{W}R_{VG}^{des} = {}^{W}R_{M2}\,{}^{M2}R_{W}^{t_0}\,{}^{W}R_{VG}^{t_0}, \tag{16} $$

the current pose of the right master ${}^{W}H_{VG}^{des}$ is

$$ {}^{W}H_{VG}^{des} = \left[\begin{array}{cc} {}^{W}R_{VG}^{des} & {}^{W}p_{VG}^{des} \\ 0 & 1 \end{array} \right]. \tag{17} $$

The current pose of the left master projected to the grasping frame ${}^{W}H_{G}^{des}$ is

$$ {}^{W}H_{G}^{des} = \left[\begin{array}{cc} {}^{W}R_{G}^{des} & {}^{W}p_{G}^{des} \\ 0 & 1 \end{array} \right], \quad \text{with} \tag{18} $$

$$ {}^{W}R_{G}^{des} = {}^{W}R_{M1}\,{}^{M1}R_{W}^{t_0}\,{}^{W}R_{G}^{t_0}. \tag{19} $$

For the controller connecting the two master devices, the pose of the virtual grasping point with respect to the left master ${}^{W}H_{\tilde{VG}}$ has to be calculated as:

$$ {}^{W}H_{\tilde{VG}} = \left[\begin{array}{cc} {}^{W}R_{\bar{VG}} & {}^{W}p_{\bar{VG}} + {}^{W}R_{\bar{VG}}ae_1 \\ 0 & 1 \end{array} \right], \tag{20} $$

with

$$ {}^{W}H_{\bar{VG}} = {}^{W}H_{G}^{des}\,{}^{W}H_{G}^{-1}\,{}^{W}H_{VG}. \tag{21} $$

The input frames ${}^{W}H_{1}$ and ${}^{W}H_{2}$ of the three spatial coupling springs A,B,C of Fig. 7 are listed in Table 2.

TABLE 2
VG Springs

Spatial Spring	${}^{W}H_{1}$	${}^{W}H_{2}$	Track
A	${}^{W}H_{G}$	${}^{W}H_{G}^{des}$	Track Γ2
B	${}^{W}H_{VG}$	${}^{W}H_{VG}^{des}$	Track Γ3
C	${}^{W}H_{\tilde{VG}}$	${}^{W}H_{VG}^{des}$	Track Γ1

As the spring's wrench output $W^{A/B/C}$ is in the frame of ${}^{W}H_{1}$, the wrench has to be transformed into base frame in order to calculate the wrench commanded to the hardware:

$$ {}^{S}W^{A} = {}^{S}\bar{T}_{W}\,{}^{W}\bar{T}_{G}\,{}^{G}W^{A}, \tag{22} $$

$$ {}^{M1}W^{A} = {}^{M1}\bar{T}_{W}\,{}^{W}\bar{T}_{G}\,{}^{G}\tilde{W}^{A}, \tag{23} $$

$$ {}^{S}W^{B} = {}^{S}\bar{T}_{W}\,{}^{W}\bar{T}_{VG}\tilde{T}\,{}^{VG}W^{B}, \tag{24} $$

$$ {}^{M2}W^{B} = {}^{M2}\bar{T}_{W}\,{}^{W}\bar{T}_{VG}\,{}^{VG}\tilde{W}^{B}, \tag{25} $$

$$ {}^{M2}W^{C} = {}^{M2}\bar{T}_{W}\,{}^{W}\bar{T}_{\tilde{VG}}\,{}^{\tilde{VG}}W^{C}, \tag{26} $$

$$ {}^{M1}W^{C} = {}^{M1}\bar{T}_{W}\,{}^{W}\bar{T}_{\tilde{VG}}\tilde{T}\,{}^{\tilde{VG}}\tilde{W}^{C}, \tag{27} $$

with $\tilde{W}^{i} = -W^{i}$. Note that transformation matrices ${}^{n}\bar{T}_{m}$ contain only rotatory elements:

$$ {}^{n}\bar{T}_{m} = \left[\begin{array}{cc} {}^{n}R_{m} & 0 \\ 0 & {}^{n}R_{m} \end{array} \right]. \tag{28} $$

The matrix $\tilde{T}$ calculates the torques resulting from the forces acting on the lever arm at a distance $(d+a)$

$$ \tilde{T} = \left[\begin{array}{ccc:c} & \mathbf{I}_3 & & \mathbf{0}_3 \\ \hdashline 0 & 0 & 0 & \\ 0 & 0 & (d+a) & \mathbf{I}_3 \\ 0 & -(d+a) & 0 & \end{array} \right]. \tag{29} $$

In the setup of [8], the rotation of the virtual pipe between the master devices (see ${}^{W}H_{G}^{des}$ and ${}^{W}H_{VG}^{des}$ in Fig. 7) has to be demanded by rotations of the master devices. In reality, the pipe can be rotated with counteracting forces at the two pipe ends. The consideration of the lever arm $(d+a)$ in $\tilde{T}$ allows the command of rotations with counteracting forces.

3.2 Passivity Proof

As discussed above, the passivity of the track is crucial for the chosen stability approach. Therefore, the energy behavior of the virtual grasping point method is discussed here. The MPMT modules of the virtual grasping point are introduced as projection subsystems PR. Note that for the ease of comprehension the PR blocks are presented separately from the track in Fig. 8 although they could be integrated into the track. Fig. 8 shows in which tracks the intrinsically passive spatial springs A-C are implemented. The PR blocks are added in track Γ1 and Γ3 such that the PI controllers of those tracks are implemented in the virtual grasping point.

The pipe can be regarded as a fixed coupling of two frames that have a distance of δH (e.g. between frame $Q = {}^{W}H_{G}^{des}$ and frame $K = {}^{W}H_{\tilde{VG}}$). The virtual coupling has been designed such that the two frames Q and K have the same orientation and lie on the same x-axis (compare equations (12)-(13)). Since a rotation of a translationally steady frame K results in a translation and rotation of frame Q, the power consistency of the force transformation is

This article has been accepted for publication in a future issue of this journal, but has not been fully edited. Content may change prior to final publication. Citation information: DOI 10.1109/TOH.2018.2809746, IEEE Transactions on Haptics

not obvious. Still, transforming the force and torque with matrix $\tilde{T}$, the passivity of the transformation is guaranteed: Considering a planar motion in the xy-plane, the power $P^{Q/K}$ in frame Q and K consists of two translational powers $P_{F_x}^{Q/K}$ and $P_{F_y}^{Q/K}$ as well as a rotational power $P_M^{Q/K}$. Thus, the power in frame Q results in

$$P_{F_x}^Q + P_{F_y}^Q + P_{M_z}^Q = F_x^Q v_x^Q + F_y^Q v_y^Q + M_z^Q \omega_z. \tag{30}$$

The consideration of the lever arm $(d+a)$ in $\tilde{T}$ ($M_z^Q = M_z^K - F_y^K(d+a)$) assures the power consistency of the virtual grasping point projection $P^Q = P^K$:

$$M_z^Q \omega_z + F_y^Q v_y^Q + F_x^Q v_x^Q = M_z^K \omega_z + F_y^K v_y^K + F_x^K v_x^K, \tag{31}$$

with $F_x^K = F_x^Q$, $v_x^K = v_x^Q$, $v_y^K = v_y^Q - (d+a)\omega_z$ and $M_z^Q = M_z^K - F_y^K(d+a)$. Analogously, the passivity of the 6-DoF kinematic transformation of subsystem PR can be proven.

Therefore, the distance a does not influence the passivity of the projection subsystem. If the springs B and C in the virtual grasping points are deflected rotationally and the distance a is increased, a potential energy is added in the spring translation. This energy input is controlled by the operator who chooses the distance a and can therefore be considered as a part of the supply rate such that the passivity condition (1) is not violated. Note that if the distance is varied during standstill of the devices (relaxed springs) the energy injection is negligible.

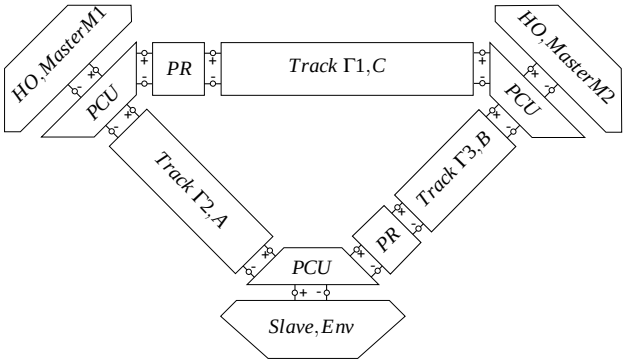

Fig. 8. Multilateral System with Virtual Grasping Point Projection

4 Task Allocation

This section introduces the Cartesian task allocation (TA) as another virtual feature providing haptic augmentation.

Consider the manipulation of a large object (e.g. a long pipe) by a human, without a telerobotic system: The right hand of the human grasping one end of the large object will be affected by the motion of the left hand grasping the pipe at another point. In case of difficult trajectories, or if high forces are necessary for the manipulation, or if not one but two humans perform the task cooperatively, it may happen that the motion of one hand influences the motion of the other hand in an undesired manner since the human may not compensate for all disturbances. This manipulation could be eased e.g. through guide rails or similar fixtures. These structures which support the human in performing the manipulation can be regarded as a non-virtual task allocation. In the case of teleoperators, the concept of task allocation allows a much broader spectrum of supporting aids to the telemanipulation. These support aids are virtual features which can augment visual and haptic perceptions.

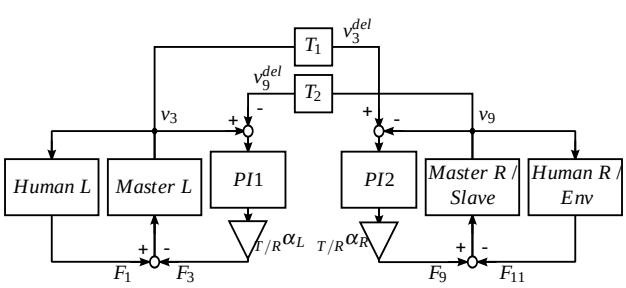

Fig. 9. Signal Flow Diagram of Position-Position Architecture with Task Allocation

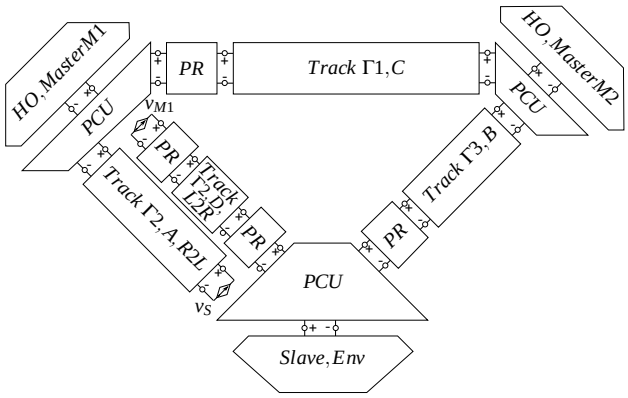

Fig. 10. Multilateral System with Virtual Grasping Point Projection and Task Allocation

The TA concept of [8] is improved here considering the coupling rigidity of slave and master M1. Furthermore, an extension that avoids constrained robot workspace configurations is proposed.

Here, the TA aims at the following distribution: The task of the right hand (master M2) is to locate the pipe end and to keep the position until the pipe is correctly oriented. The task of the left hand (master M1) is the reorientation of the pipe. A task allocation is designed here which decouples the translational motion of the pipe end from the left hand input such that the right hand feels no forces (but torques) caused by the left hand motion. Thus, the control of the pipe end is decoupled from unintentional commands of the left hand and other disturbances.

4.1 Implementation

Similar to the method proposed in [7], the task allocation can be implemented by parameters $\alpha_{M1/M2}$ that scale the stiffness and the damping of the PI-controller or its force and torque feedback:

$$_{T/R}\alpha_{M1/M2} \in [0,1], \tag{32}$$

$$_{T/R}\alpha_{M2} = 1 - {}_{T/R}\alpha_{M1}. \tag{33}$$

The scaling ${}_T\alpha$ acts on the forces (translation T) sent from the left or right master $M1/M2$. ${}_R\alpha$ acts on the torques (rotations R). Fig. 9 presents a general PP-architecture with task allocation scaling. Note that the human may be positioned distantly from the slave. In a bimanual setup with one operator, the delay between the master devices is zero and ${}_{T/R}\alpha_L = {}_{T/R}\alpha_{M2}$ and ${}_{T/R}\alpha_R = {}_{T/R}\alpha_{M1}$. In the master-slave coupling tracks, the master side scaling ${}_{T/R}\alpha_L = 1$

This article has been accepted for publication in a future issue of this journal, but has not been fully edited. Content may change prior to final publication. Citation information: DOI 10.1109/TOH.2018.2809746, IEEE Transactions on Haptics

and ${}_{T/R}\alpha_R = {}_{T/R}\alpha_{M1}$ for master M1 and ${}_{T/R}\alpha_R = {}_{T/R}\alpha_{M2}$ for master M2. To obtain a DoF-specific Cartesian task allocation it is crucial that these PI controllers operate in the VG as the task allocation is designed in the VG. Therefore, two PR blocks need to be added to track Γ2 as depicted in Fig. 10. In [8], the spatial springs of tracks Γ2 and Γ3 are positioned in the virtual grasping point. Therefore, the slave is coupled to two distant controllers which leads to higher flexibility in the translational DoFs and thus reduces the position accuracy. Here, in order to improve the coupling rigidity, it is proposed to split the track Γ2 into two directions of flow. Such that the PI of the *R2L*-part (which determines the force feedback to master M1) can provide a direct coupling between slave and master M1 in the grasping point G. This is possible as the slave feedback to master M1 is not affected by the TA and therefore doesn't have to be calculated in the VG. Thus, the coupling rigidity is increased such that the master M2 tracks the slave position better. The controller of the *L2R*-part remains in the virtual grasping point to assure the task allocation functionality.

In contrast to the spring setup in Section 3 and to the task allocation design of [8], this new task allocation concept requires four coupling springs A-D (compare Table 3). The spring D is located in the virtual grasping point VG and spring A remains in the grasping point.

TABLE 3
TA Springs

Spatial Spring	${}^{W}H_1$	${}^{W}H_2$	Track
A	${}^{W}H_G$	${}^{W}H_G^{des}$	Γ2 *R2L*
D	${}^{W}H_{VG}$	${}^{W}H_{\tilde{VG}}$	Γ2 *L2R*

The feedback forces of the springs change:

$$ {}^{S}W^{A} = [0 \;\; 0 \;\; 0 \;\; 0 \;\; 0 \;\; 0]^{T} \tag{34} $$

$$ {}^{M1}W^{A} = {}^{M1}\overline{T}_{W}\,{}^{W}\overline{T}_{G}\,{}^{G}\tilde{W}^{A}, \tag{35} $$

$$ {}^{S}W^{B} = {}^{S}\overline{T}_{W}\,{}^{W}\overline{T}_{\tilde{VG}}\tilde{T}\,\kappa^{RC}\kappa_{M2}^{TA}\,{}^{VG}W^{B}, \tag{36} $$

$$ {}^{M2}W^{B} = {}^{M2}\overline{T}_{W}\,{}^{W}\overline{T}_{VG}\,\kappa^{RC}\,{}^{VG}\tilde{W}^{B}, \tag{37} $$

$$ {}^{M2}W^{C} = {}^{M2}\overline{T}_{W}\,{}^{W}\overline{T}_{\tilde{VG}}\,\kappa^{RC}\kappa_{M1}^{TA}\,{}^{\tilde{VG}}W^{C}, \tag{38} $$

$$ {}^{M1}W^{C} = {}^{M1}\overline{T}_{W}\,{}^{W}\overline{T}_{\tilde{VG}}\tilde{T}\,\kappa^{RC}\kappa_{M2}^{TA}\,{}^{\tilde{VG}}\tilde{W}^{C} \tag{39} $$

$$ {}^{S}W^{D} = {}^{S}\overline{T}_{W}\,{}^{W}\overline{T}_{VG}\kappa_{M1}^{TA}\tilde{T}\,{}^{VG}W^{D}, \tag{40} $$

$$ {}^{M1}W^{D} = [0 \;\; 0 \;\; 0 \;\; 0 \;\; 0 \;\; 0]^{T}. \tag{41} $$

The matrices κ^{RC} will be used to reduce the right robot's workspace limitations in the next step but can be first assumed to be equal to the unity matrix $\mathbf{I}_6 \in R^{6x6}$. The multi-DoF task allocation can be implemented through the matrices κ_{M1}^{TA} and κ_{M2}^{TA}

$$ \kappa_{M1}^{TA} = \begin{bmatrix} {}_{T}\alpha_{M1}\mathbf{I}_3 & \mathbf{0}_3 \\ \mathbf{0}_3 & {}_{R}\alpha_{M1}\mathbf{I}_3 \end{bmatrix} \tag{42} $$

and

$$ \kappa_{M2}^{TA} = \begin{bmatrix} {}_{T}\alpha_{M2}\mathbf{I}_3 & \mathbf{0}_3 \\ \mathbf{0}_3 & {}_{R}\alpha_{M2}\mathbf{I}_3 \end{bmatrix}, \tag{43} $$

with the zero matrix $\mathbf{0}_3$ and the unity matrix $\mathbf{I}_3 \in R^{3x3}$.

In the chosen scenario, the translational task allocation factors should be chosen as follows:

$$ {}_{T}\alpha_{M2} \in [0.7, 1], \tag{44} $$

$$ {}_{T}\alpha_{M1} = 1 - {}_{T}\alpha_{M2}. \tag{45} $$

If only master M1 would control the rotations, the translations in the right hand could be disturbed by unexpected rotational motions in the operator's right hand. Therefore, the rotational task allocation values remain unaltered (${}_{R}\alpha_i = 0.5$) for now. The feedback from slave to the masters is not scaled since the slave's motion should always be correctly perceived at the master devices.

4.2 Robot Workspace Limitations

Especially in robots with serial kinematics, the workspace is constrained by singularities and dynamic nonlinearities. These issues can negatively affect the precision and smoothness of motion when large motions are required. The presented setup might have limited workspace depending on the robots' configuration.

To reduce these effects, the orientation of the master device M2 can be decoupled from the pipe orientation such that it is able to change its orientation freely. This leads to a variety of M2 configurations such that singularities or other limitations can be avoided. Master M2 can then still be used to control the translations of the pipe end. The only drawback is that this robot can then set a desired orientation only through forces in cooperation with the second input device and not through torques. The torques of the controllers coupling the right master to the other devices can be set to zero to achieve this behavior. Therefore ${}_{T}\kappa^{RC}$ has to be chosen as:

$$ {}_{T}\kappa^{RC} = \begin{bmatrix} \mathbf{I}_3 & \mathbf{0}_3 \\ \mathbf{0}_3 & \mathbf{0}_3 \end{bmatrix}. \tag{46} $$

4.3 Passivity Discussion

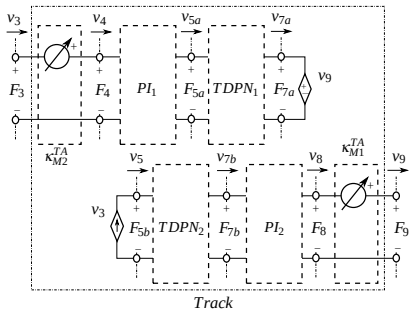

Fig. 11. Network Representation of the PP-architecture of Track Γ1 with Task Allocation

In the MPMT, the allocation factors κ_{M2}^{TA} and κ_{M1}^{TA} can be designed as dependent power sources (compare Fig. 11) with direction depending energy behavior [25] such that the power P_{P4} and P_{P8} are reduced by the task allocation factors ($0 \leq {}_{T/R}\alpha_{M1/M2} \leq 1$) in R2L and L2R direction respectively:

$$ P_{P3}(t) = {}_{T/R}\alpha_{M2}P_{P4}(t) = v_4(t)\,{}_{T/R}\alpha_{M2}F_4(t), \tag{47} $$

$$ P_{P9}(t) = {}_{T/R}\alpha_{M1}P_{P8}(t) = v_8(t)\,{}_{T/R}\alpha_{M1}F_8(t). \tag{48} $$

For example, the power source κ_{M2}^{TA} in the *R2L* part of the track has an effect only in *R2L* direction. In this direction, it has a dissipating characteristic. In contrast, the same power source

This article has been accepted for publication in a future issue of this journal, but has not been fully edited. Content may change prior to final publication. Citation information: DOI 10.1109/TOH.2018.2809746, IEEE Transactions on Haptics

κ_{M2}^{TA} has an energy generating behavior in $L2R$ direction but the injected energy is dissipated by the dependent flow source v_9 and thus, is not transmitted to the right part of the track. This holds analogously for the power source κ_{M1}^{TA}.

5 Time Delay

If the communication channel has a time delay, energy is produced by the TDPN subsystem representing the communication link which may lead to instability. Concerning literature on multilateral systems, the issue of time delay is addressed in [7] and [26] applying the TDPA, whereas, wave variable transformation method has been followed in [6] and [27]. A closer analysis of the effects of time delay in different types of cooperative control methods in MMMS systems is carried out in [28]. A trilateral system with bounded time delay is introduced in [29] where the system stability is studied through an appropriate Lyapunov like function. Here, it is presented, how the TDPA [17], [23], [30] can be integrated into the multilateral multi-DoF structure in combination with the haptic augmentation concepts. The

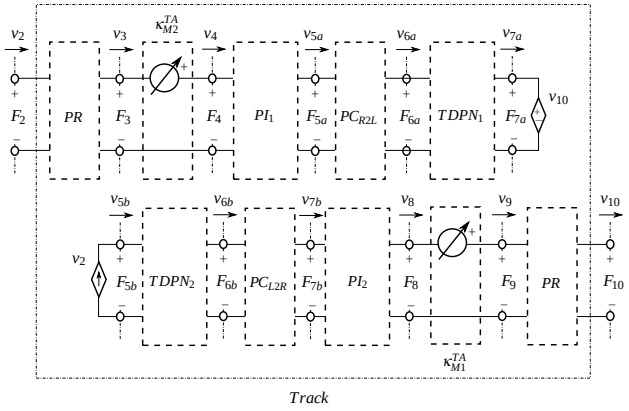

Fig. 12. Network Representation of the PP-architecture with Task Allocation and Passivity Controlled Communication Channel

TDPA provides passivity observers (PO) and passivity controllers (PC). The positions of the PCs in the track containing PR and TA subsystems are depicted in Fig. 12. The POs measure the energies flowing in the respective directions at the ports of the TDPN subsystems. Thus, the energy generation of the system can be analyzed. If the observed TDPN has generated energy, the corresponding passivity controller preserves $\mathscr{L}_2$-stability through the dissipation of the excessive energy. The POs are located at ports 6a and 7a (R2L) and ports 5b and 6b (L2R) respectively such that the energy generated in the TDPNs can be measured. Two PCs added next to $TDPN_1$ and $TDPN_2$ dissipate this energy in the corresponding direction of energy flow. In the PP architecture, admittance type PCs are used that alter the velocity fed to the PI controllers.

In case of time delay, the passivity condition (2) has to be reformulated:

$$\begin{aligned} &E^{L,TDPN_1}(t)+E^{R,TDPN_1}(t)=E_{in}^{L,TDPN_1}(t-T_1)\\ &-E_{out}^{R,TDPN_1}(t)+E_{in}^{R,TDPN_1}(t-T_2)-E_{out}^{L,TDPN_1}(t)\geq 0 \end{aligned} \tag{49}$$

and split up into

$$E_{in}^{L,TDPN_1}(t-T_1)-E_{out}^{R,TDPN_1}(t)\geq 0, \tag{50}$$

$$E_{in}^{R,TDPN_1}(t-T_2)-E_{out}^{L,TDPN_1}(t)\geq 0. \tag{51}$$

Thus it is sufficient if e.g, PC_{R2L} dissipates the observed time delayed energy difference E_{obs}:

$$E_{obs}^{R2L,TDPN_1}=E_{in}^{R,TDPN_1}(t-T_1)-E_{out}^{L,TDPN_1}(t). \tag{52}$$

The velocity v_{PC}^{R2L} which is generated by the admittance type PC_{R2L} and sent to the left side PI_1 in a sum with v_{6a} is then calculated as follows:

$$v_{PC}^{R2L}(t)=-\frac{E_{obs}^{R2L,TDPN_1}(t)}{\Delta T F_{6a}^2(t)}F_{6a}(t).$$

The admittance type PC based TDPA can be integrated into the multi-DoF structure as follows: The pose vector r with three positions and three angles respectively can be calculated from the components p, R of the homogeneous transformation matrix H:

$$r=\begin{bmatrix} p \\ \omega\Theta \end{bmatrix},$$

with the angle-axis representation $\omega\Theta$ that can be calculated from the rotation matrix R:

$$\Theta=arccos(\frac{tr(R)-1}{2}),$$

$$\omega=\frac{1}{2sin(\Theta)}\begin{bmatrix} {}^iR_{3,2}-{}^iR_{2,3} \\ {}^iR_{1,3}-{}^iR_{3,1} \\ {}^iR_{2,1}-{}^iR_{1,2} \end{bmatrix}.$$

The elements of the pose vector r can be passivity controlled separately, resulting in a new pose vector r^{PC}. The matrix H^{PC} fed to the spatial spring can be found from the passivity control output via Rodrigues' rotation formula:

$$\mathbf{R}^{PC}=\mathbf{I}+sin(\Theta^{PC})[\omega^{PC}]_x+(1-cos(\Theta^{PC}))[\omega^{PC}]_x\otimes[\omega^{PC}]_x,$$

where $[\omega^{PC}]_x$ is the skew symmetric cross product matrix of the axis vector ω^{PC}.

The effects of the TDPA and the delay itself on transparency is discussed in the experiments in Section 6. In [31], it was shown that the TDPA provides good performance compared to other frequently used methods. Due to the modular structure of the MPMT, the wave variables method can also be applied.

6 Experiments

In this chapter, the proposed multilateral system will be analyzed experimentally with focus on the virtual grasping point and the task allocation. The DLR HUG which consists of two redundant 7 DoF light weight robots served as the bimanual haptic input device (see Fig. 2). The left arm of the humanoid robot DLR SpaceJustin (see Fig. 1) has been used as the single slave device.

The DLR Hit hand (Wessling Robotics) was used as the tool to grasp the pipe. The CyberGlove (CyberGlove Systems) served as the hand interface. The grasped pipe was a light plastic pipe made of polypropylene. The human operator could see the environment of DLR SpaceJustin through the robot's stereo cameras via a head-mounted display.

All robots have been linked using the position-position teleoperation scheme and no force sensors have been applied in the control loop although endeffector FTS have been used on all devices for measuring interaction forces. The controller constants have been chosen as depicted in Table 4 (rotational and translational damping B_i and stiffness K_i). No local damping has been applied. To tune each coupling controller, only the respective track was activated. The controller spring (I-gain of the controller) was tuned

This article has been accepted for publication in a future issue of this journal, but has not been fully edited. Content may change prior to final publication. Citation information: DOI 10.1109/TOH.2018.2809746, IEEE Transactions on Haptics

TABLE 4
Control Parameters

Track	K_T [N/m]	B_T [Ns/m]	K_R [Nm/rad]	B_R [Nms/rad]
Γ 1	400	3	15	1
Γ 2	300	6	10	0.45
Γ 3	300	6	10	0.45

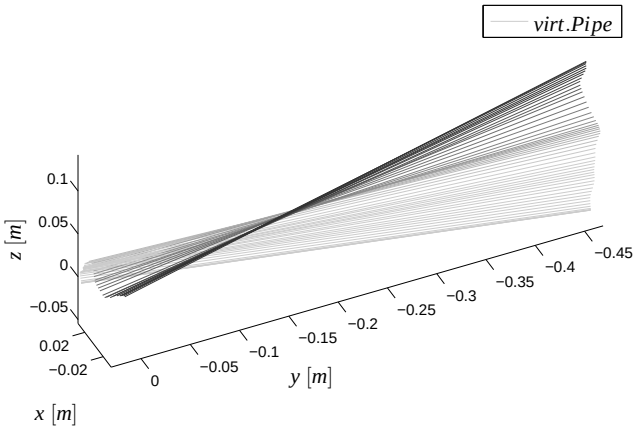

Fig. 13. Exp1a: Virtual Pipe Motion in a Bilateral Master-Master Setup without Task Allocation (Devices M1, M2 and Track Γ1)

to achieve a stiff coupling. The passivity analysis of Section 3 and 4 assuming a continuous time system does not limit the controller stiffness but only requires a positive semi-definite damping. The damping (P-gain of the controller) was set to counterbalance the destabilizing effects of discretization. This damping is necessary, independent of the stability approach (passivity, Routh-Hurwitz etc.) being used. Therefore, the passive track design does not lead to high conservatism and promises good performance w.r.t. transparency measures as position error and transmitted impedances between the coupled devices. In contrast, the time delay control approach affects the control gains through an adaptive damping. Therefore, the transparency is mainly reduced in case of a delay in the communication channels. Still, the TDPA promises good performance in delayed coupled systems compared to other time delay control methods [31].

The first experiment Exp1 focuses the application in virtual environments. Therefore, the bilateral link with virtual pipe coupling between master M1 and master M2 (Track Γ1) is analyzed. A rotation around the pipe end at master M2 is performed. The performance with (Exp1b) and without task allocation (Exp1a) is compared. Fig. 13 (pipe color indicates time) depicts the motion of the virtual pipe without task allocation. The virtual pipe represents the link of ${}^{W}H_{G}^{des}$ and ${}^{W}H_{VG}^{des}$. Master M1 rotates around master M2 which tries to fix its initial position on the left hand side of the plot. The computed PI controller forces F^{comp} that are demanded from the robots have opposite signs for master M1 and master M2 (compare Fig. 14). The force values F^{meas} measured by the force sensor differ, as the operator hands have to counteract e.g. against the link masses. The task allocation is activated for Fig. 15. The task allocation values have been chosen as noted in Table 5 (bilateral case). It is obvious that master M2 can maintain its translational position more easily if the task allocation is active.

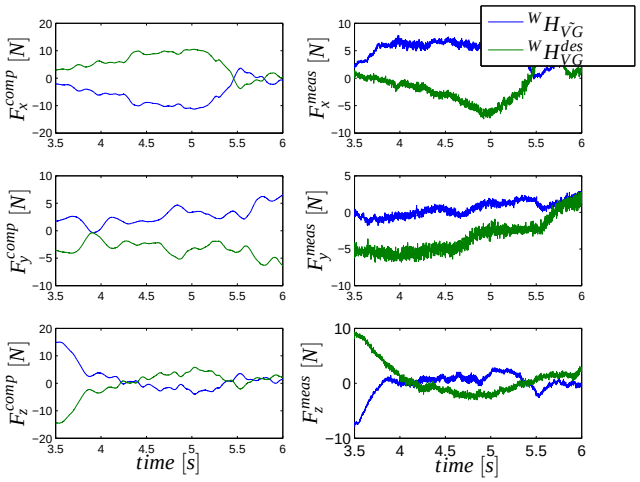

Fig. 14. Exp1a: Measured and Computed Forces in a Bilateral Master-Master Setup without Task Allocation (Devices M1, M2 and Track Γ1)

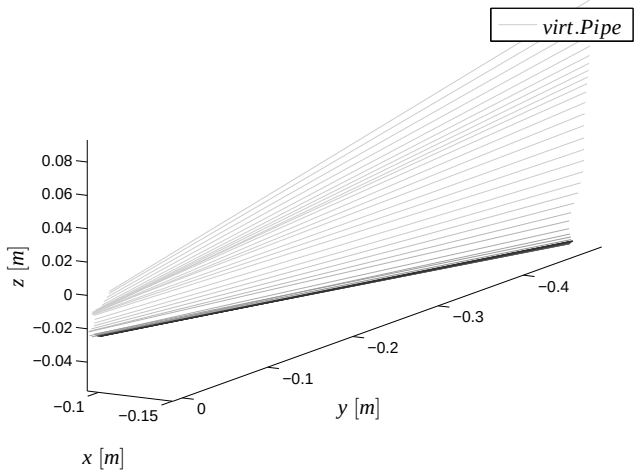

Fig. 15. Exp1b: Virtual Pipe Motion in a Master-Master Bilateral Setup with Task Allocation (Devices M1, M2 and Track Γ1)

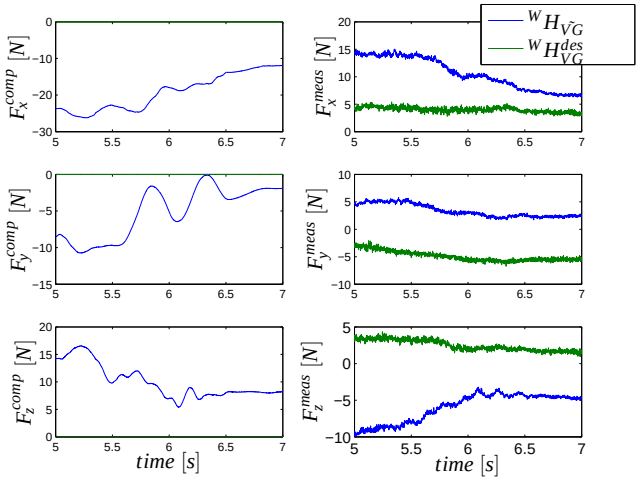

Fig. 16. Exp1b: Measured and Computed Forces in a Bilateral Master-Master Setup with Task Allocation (Devices M1, M2 and Track Γ1)

This article has been accepted for publication in a future issue of this journal, but has not been fully edited. Content may change prior to final publication. Citation information: DOI 10.1109/TOH.2018.2809746, IEEE Transactions on Haptics

TABLE 5
Task Allocation Settings for Bilateral and Multilateral Experiments

α bilateral	Value	α multilateral	Value
${}_T\alpha_{M1}$	0	${}_T\alpha_{M1}$	0.3
${}_R\alpha_{M1}$	0.5	${}_R\alpha_{M1}$	0.5
${}_T\alpha_{M2}$	1	${}_T\alpha_{M2}$	0.7
${}_R\alpha_{M2}$	0.5	${}_R\alpha_{M2}$	0.5

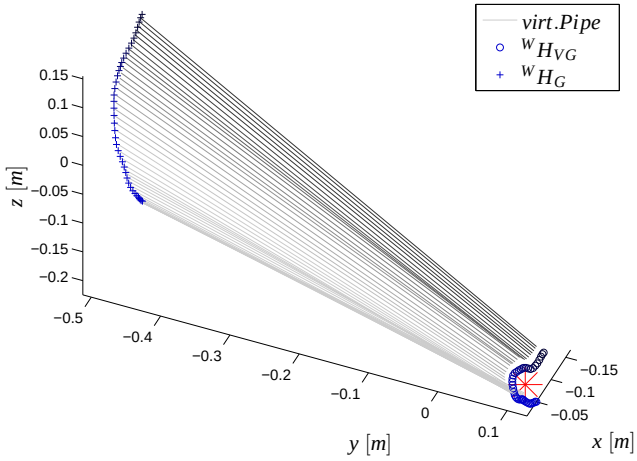

Fig. 17. Exp2a: Virtual Pipe Motion in a Bilateral Master-Slave Setup (Devices M1, S and Track Γ2)

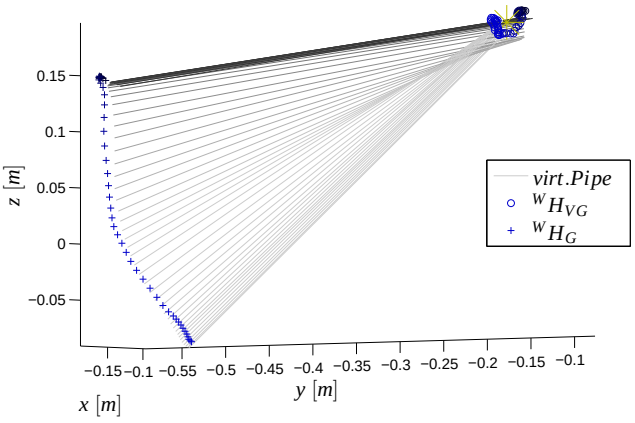

Fig. 18. Exp2b: Virtual Pipe Motion in a Multilateral Setup without Task Allocation (Devices M1, M2, S and Tracks Γ1, Γ2 and Γ3)

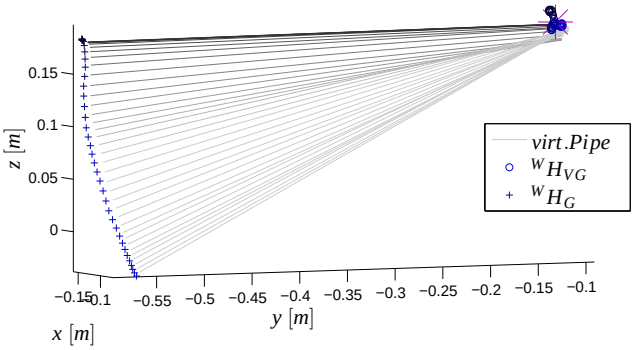

Fig. 19. Exp2c: Virtual Pipe Motion in a Multilateral Setup with Task Allocation (Devices M1, M2, S and Tracks Γ1, Γ2 and Γ3)

Fig. 16 shows that all the forces F^{comp} sent to master M2 are canceled if task allocation is active. The measured forces F^{meas} at master M2 side are constant during the rotational procedure as the right operator hand does not need to resist against the left hand's demand (${}_T\alpha_{M1} = 0$). Comparing Fig. 14 and Fig. 16, one can see that in order to rotate the pipe, the right hand at master M2 has to act with a force F_z^{meas} against the rotation only if the task allocation is not active.

The next set of experiments Exp2 compares the steadiness of the pipe end during rotation around the pipe end. In the first part Exp2a (see Fig. 17), a bilateral system with direct coupling between master M1 and slave (Track Γ2) is evaluated. As the rotational position following of master M1 and slave is not optimal, the resulting translational position error in the pipe end is high. The average position of the pipe end is depicted with a star shape.

In the next step (Exp2b), the track Γ3 is activated such that a real multilateral coupling as depicted in Fig. 8 can be evaluated in Fig. 18. The task allocation is not active. As the additional coupling via track Γ3 makes the system stiffer, especially the slave's position following is improved compared to Fig. 17.

Comparing the rotational accuracy in experiments Exp2a to Exp2b, the mean value $meanVG^0$ of distance from pipe end position VG (${}^W H_{VG}$) to the initial pose of pipe end position S (${}^W H_{VG}(t_0)$) is lower for Exp2b with virtual grasping point ($meanVG^0(Exp2a) = 0.0201$, $meanVG^0(Exp2b) = 0.0099$). This shows that the PE steadiness can be improved using bimanual control.

For experiment Exp2c, the task allocation is activated and the track Γ2 is split in to parts corresponding to Fig. 10. Thus, the position of the pipe end is more steady in Fig. 19. The task allocation values have been chosen as in Table 5 (multilateral case) which, when subjectively evaluated, resulted in the best performance. Because of cross couplings caused by the available robot workspace, the task allocation was chosen such that master M1 gained 30% authority (${}_T\alpha_{M1} = 0.30$) on the pipe end's translational motion. Comparing Fig. 18 and Fig. 19 one can see that the steadiness of the pipe end during reorientation is slightly more precise if task allocation is active. Another benefit of the task allocation is that the workload of the operator may be reduced, as he needs to apply less forces for the desired motions. Comparing the rotational accuracy in experiments Exp2b and Exp2c, the mean value $meanVG$ of distance between Master M_2 (${}^W H_{VG}^{des}$) and VG (${}^W H_{VG}$) is clearly lowest for Exp2c with task allocation ($meanVG(Exp2b) = 0.00533$, $meanVG(Exp2c) = 0.00162$). Still, only in a user study, the performance can be evaluated reliably.

The next set of experiments (Exp3) presents a procedure with rotation in the xy-plane around the virtual grasping point with subsequent plug-in of the pipe into a hole. This experiment with contact forces has been performed in a bilateral setup (direct Master 1 - Slave coupling, Fig. 20 and Fig. 21) as well as in a multilateral setup with task allocation (Tracks Γ1, Γ2 and Γ3, Fig. 22 and Fig. 23). The respective pipe motion plots show that the plug-in is difficult in the bilateral case (see Fig. 21). In contrast, only one plug-in attempt is necessary with the multilateral setup (see Fig. 23). The computed forces resulting from one spatial

This article has been accepted for publication in a future issue of this journal, but has not been fully edited. Content may change prior to final publication. Citation information: DOI 10.1109/TOH.2018.2809746, IEEE Transactions on Haptics

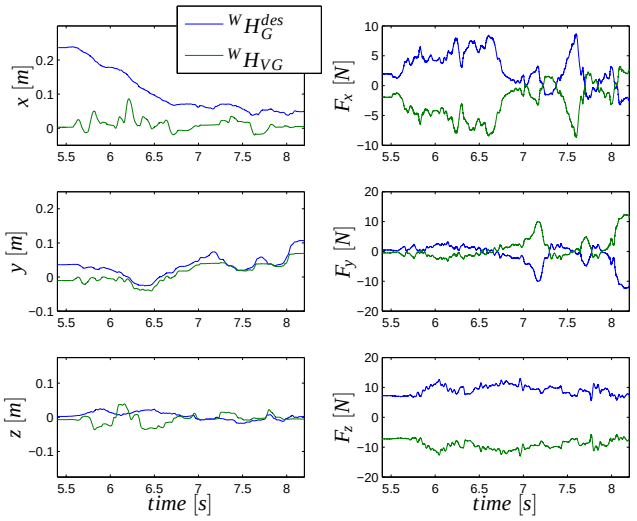

Fig. 20. Exp3a: Position and Forces during Plug-In Procedure in a Bilateral Master-Slave Setup (Devices M1, S and Track Γ2)

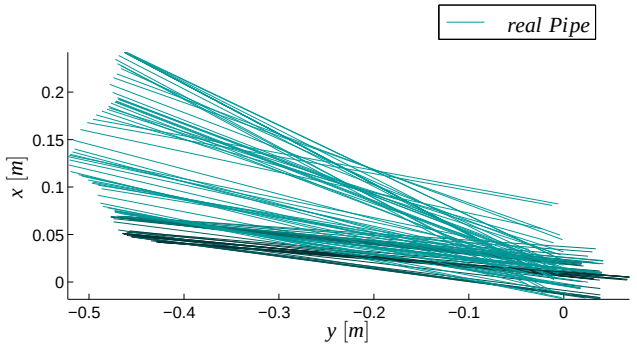

Fig. 21. Exp3a: Pipe Motion during Plug-In Procedure in a Bilateral Master-Slave Setup (Devices M1, S and Track Γ2)

spring in the unimanual setup (depicted in Fig. 20) clearly present three contacts with the wall (compare F_y). Due to the three coupling springs in the bimanual setup, the force feedback consists not only from the spring deflections resulting from the slave's contact but also from the coupling via the virtual grasping points. Still, the contact forces in y-direction can be recognized in both master devices.

A time delay is considered in the last experiment (Exp4, see Fig. 24 and 25). The system had been tuned at the verge of stability at 10ms roundtrip delay. The slave is assumed to be located distant from the master devices such that the tracks Γ2 and Γ3 contain a roundtrip delay of 40ms. Fig. 24 depicts the plug-out motion of the pipe (Fig. 25 8.7s-9.5s). Fig. 25 shows that the position tracking quality of the three devices during the plug-in and plug-out motion is satisfactory despite time delay. Besides the inevitable latency effects, the delay and the application of the TDPA do not reduce performance in terms of position error of desired and actual position drastically.

7 User Study

In the following study we tried to answer two hypotheses:

- H1: The proposed bimanual control approach allows a higher level of accuracy while performing a rotational position matching task compared to unimanual control.

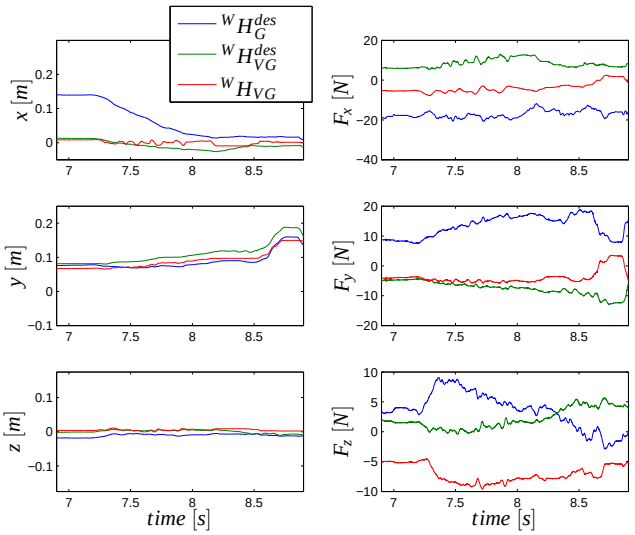

Fig. 22. Exp3b: Position and Forces during Plug-In Procedure in a Multilateral Setup with Task Allocation (Devices M1, M2, S and Tracks Γ1, Γ2 and Γ3)

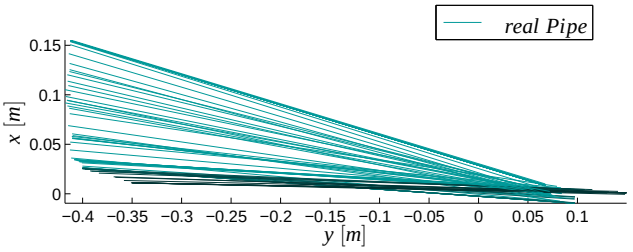

Fig. 23. Exp3b: Pipe Motion during Plug-In Procedure in a Multilateral Setup with Task Allocation (Devices M1, M2, S and Tracks Γ1, Γ2 and Γ3)

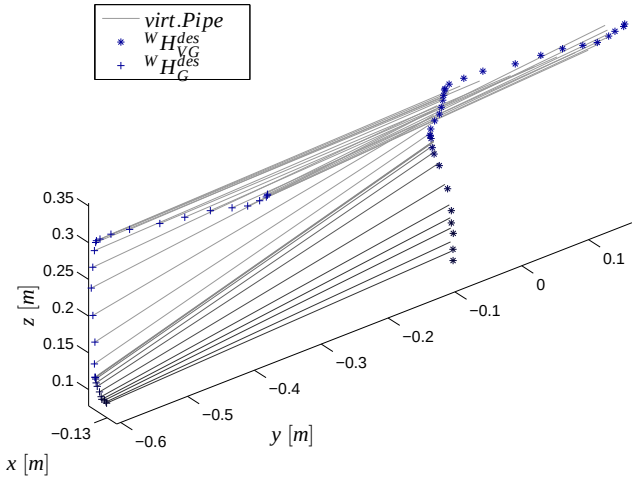

Fig. 24. Exp4: Pipe Motion with 40ms Roundtrip Delay in a Multilateral Setup with Task Allocation (Devices M1, M2, S and Tracks Γ1, Γ2 and Γ3)

This article has been accepted for publication in a future issue of this journal, but has not been fully edited. Content may change prior to final publication. Citation information: DOI 10.1109/TOH.2018.2809746, IEEE Transactions on Haptics

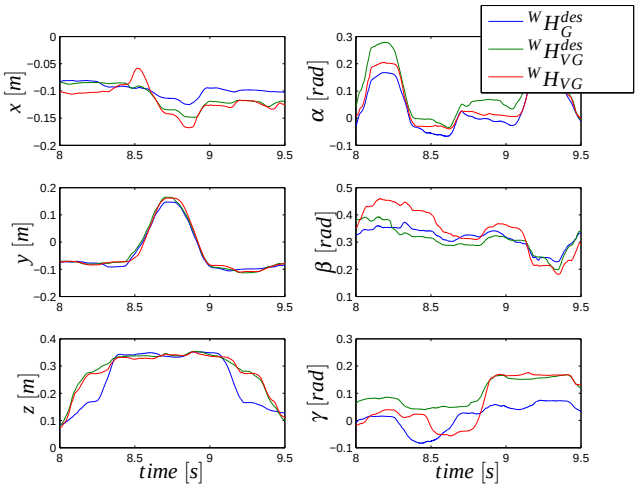

Fig. 25. Exp4: Position Tracking with 40ms Roundtrip Delay in a Multilateral Setup with Task Allocation (Devices M1, M2, S and Tracks Γ1, Γ2 and Γ3)

- H2: In case of bimanual control, the task allocation approach should lead to higher accuracy compared to an approach without task allocation.

Besides the mental and physical workload in the bimanual setup, the performance in terms of accuracy is evaluated in the user study. Since the proposed concepts promise an increase in rotational accuracy and since the perception of slave contacts with the environment is not decreased (compare experiment set 3), this user study focuses on rotational positioning tasks.

7.1 Method

The user study was conducted with N=10 participants (9 male, 1 female) in the age group between 23 and 35 years (M=28.9; SD=4.1). A within subject design has been chosen such that each participant had to perform the task set with each condition. For the sake of experimental control and to reduce undesired effects (e.g. workspace limitations, singularities) of the robot hardware as far as possible, the study was performed with the HUG and a virtual reality instead of a slave robot such that only track Γ1 was activated. This coupling of master M1 and master M2 reflects the whole functionality of the virtual grasping point concept. Furthermore, the design in the virtual reality allowed clearer instructions and thus, a more detailed evaluation of separate tasks was possible.

7.1.1 Technical Setup

The controller of the DLR HUG was implemented in Matlab Simulink and executed on a RTLinux system. A pedal served as a deadman switch to activate the robot power. The Instant Player [32] was applied to present the virtual reality to the user. The participants saw the virtual scene on the head mounted display (HMD) nVisorSX60.

7.1.2 Task

A set of ten tasks had to be performed with each condition. The virtual reality showed two pipes (see Fig. 26). The gray pipe was controlled by the operator. The second red transparent pipe presented the desired pose of the pipe. When the desired pose was reached, the color of the transparent pipe turned from red to green.

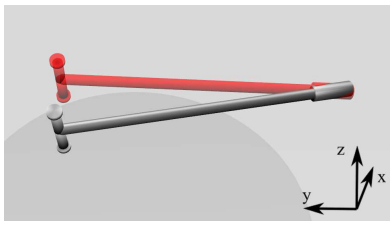

Fig. 26. Virtual Reality Scene of User Study

After half a second in the desired pose, a new desired pipe pose appeared in red color. The pipe poses have been chosen such that the pipe had to be rotated around the pipe end. The study focuses on the positioning accuracy of different control setups. No contacts with the environment are considered since the main performance increase through the proposed haptic augmentation concept is expected in the accurate orientating of the object also without contact. Furthermore, in the experimental section it was shown that the performance with contact is not decreased compared to standard telemanipulation.

7.1.3 Experimental Design

Three conditions have been chosen for the user study:

- Condition 1: unimanual control without haptic augmentation
- Condition 2: bimanual control with virtual grasping point coupling and without task allocation
- Condition 3: bimanual control with virtual grasping point and with task allocation

The participants started with a training procedure with a condition sequence 1,2,3 to understand the differences of the approaches properly. The order of conditions was randomized for the test subjects to control time effects as fatigue and training.

Another training phase was performed before the accounted task in the respective condition. The task set started from a unique initial position. The test subjects were instructed to maintain the pipe end position during the motion of the pipe to the desired position. In addition, the examiner informed that the retention of the pipe end position during the task had higher priority than the time needed for task completion.

Furthermore, the test subjects completed a demographic and an immersive tendency questionnaire [33] to identify correlations with the related performance. Additionally, after the user study a simulator sickness questionnaire [34] had to be filled.

7.2 Results

The simulator sickness questionnaire indicated that no test subject had to be excluded from the analysis. The following measures have been evaluated:

- The time t in [s] needed for one task
- The translational path $path_{PE}$ in [m] of the pipe end
- The root mean square of the pipe end's translational velocity $RMS(V_{PE})$ in [m/s]
- The root mean square of the translational difference of desired and actual pipe end position $RMS(P_{PE}^{diff})$ in [m]
- The absolute maximum of the translational difference of desired and actual pipe end position $MAX(|P_{PE}^{diff}|)$ in [m]

- user workload

The $RMS(V_{PE})$ and the $path_{PE}$ should be close to zero, since the translational position of the desired pipe end is steady throughout the experiment. Also the measures $RMS(P_{PE}^{diff})$ and $MAX(|P_{PE}^{diff}|)$ should be low in the best approach. Note that orientation errors are not explicitly analyzed since the path of the pipe to the desired position could be chosen without restrictions.

The resulting mean value and standard deviation in brackets are presented in Table 6. The dimensions x,y and z can be analyzed in Fig. 26.

TABLE 6
Results

	Condition		
	1	2	3
Mental Workload	12.5 (2.80)	10.6 (2.59)	9.6 (2.76)
Physical Workload	11.0 (3.06)	10.5 (3.41)	8.9 (2.13)
t	7.29 (2.11)	6.60 (2.30)	6.18 (1.36)
$path_{PE}$	0.541 (0.078)	0.219 (0.069)	0.233 (0.061)
	x-dimension		
$RMS(V_{PE})$	0.064 (0.006)	0.0277 (0.005)	0.0314 (0.006)
$RMS(P_{PE}^{diff})$	0.0288 (0.006)	0.0192 (0.003)	0.0182 (0.004)
$MAX(\|P_{PE}^{diff}\|)$	0.0635 (0.011)	0.0347 (0.008)	0.0342 (0.007)
	y-dimension		
$RMS(V_{PE})$	0.017 (0.002)	0.0106 (0.001)	0.0113 (0.001)
$RMS(P_{PE}^{diff})$	0.0109 (0.002)	0.0115 (0.002)	0.0122 (0.003)
$MAX(\|P_{PE}^{diff}\|)$	0.0208 (0.003)	0.0188 (0.004)	0.0205 (0.004)
	z-dimension		
$RMS(V_{PE})$	0.0763 (0.012)	0.028 (0.004)	0.030 (0.006)
$RMS(P_{PE}^{diff})$	0.0351 (0.005)	0.0260 (0.001)	0.0241 (0.002)
$MAX(\|P_{PE}^{diff}\|)$	0.0721 (0.012)	0.0423 (0.005)	0.043 (0.005)

The main assumptions for repeated measures ANOVA (rmANOVA), i.e. normality of residuals and sphericity were tested by Shapiro-Wilk's test and Mauchly's test. Only violations of these assumptions are reported in the following analyses. In the case of non-normality, the non-parametric Friedman test was chosen. In a first step, the effect of experimental conditions on average completion times t were analyzed in rmANOVA with condition as within factor. Results indicate no significant effect of condition (F (2, 18) = 1.4, n.s.). Next, the average path lengths ($path_{PE}$) were explored. Since data were not distributed normally for this variable in condition 1 (Shapiro-Wilk's W = .84; $p < .05$), a Friedman test was performed. The results show a highly significant effect of condition, p = .001. In subsequent Wilcoxon tests, we found significant differences between condition 1-2 as well as 1-3 (both $ps < .01$), but no significant difference between condition 2-3.

Regarding the empirical distributions for RMS of velocity ($RMS(V_{PE})$) for the three dimensions and conditions also indicated non-normality in four different factor combinations. Thus, three independent Friedman tests with condition as within variable were computed for each dimension. For the x-dimension the Friedman test revealed a significant effect of conditions ($p <.001$). Contrasting the conditions in Wilcoxon tests showed significant differences between 1-2 as well as 1-3 (both $ps < .01$) and a non-significant difference between 2-3 (p = .058). The very same result was found for the y-dimension. Significance was also reached in a Friedman test analyzing data of the z-dimension (p = .001). Here, only the contrasts between 1-2 as well as 1-3 reached significance in Wilcoxon's test (both $ps < .01$).

The data for RMS of the position error ($RMS(P_{PE}^{diff})$) also violated the assumption of normality. Again the above result pattern was evident for the x- and the z-dimension with significant Friedman tests (both $ps < .01$) and significant differences between 1-2 and 1-3 (all $ps \leq .01$). Yet, no significant result was found for the y-dimension.

Finally, we performed a rmANOVA on the maximum absolute position error ($MAX(|P_{PE}^{diff}|)$) with dimension and condition as within factors. Testing sphericity with Mauchly's procedure indicated a violation of the assumption in the condition factor (Mauchly's W = .40; $p < .05$) and the Dimension * Condition interaction (Mauchly's W = .04; $p < .01$). Thus the Greenhouse-Geisser correction was applied in these cases. dimension and condition main effects were highly significant (F (2, 18) = 165.1, $p <.001$ and F (1.25,11.23) = 63.2, $p <.001$) as well as the interaction of both factors (F (2.28,20.48) = 35.4, $p <.001$). Pairwise comparisons with Bonferroni correction show that results for all three dimensions differ significantly (all $ps < .01$) and that conditions 1-2 and 1-3 differ significantly (both $ps < .001$). The Dimension * Condition Interaction is mainly due to the results for the y-dimension; here no substantial differences between the conditions are evident in contrast to the x and z-dimension. Next, the mental workload ratings were analyzed. Data were not distributed normally in condition 2 (Shapiro-Wilks W = .83; $p <.05$) and hence Friedmans test was performed. Yet, results yielded no significant differences between the conditions. Finally, we performed a rmANOVA on the physical load ratings with condition as within factor. Results showed no significant effect (F (2, 18) = 1.96, n.s.).

7.3 Discussion

Overall, the results indicate that the test subjects showed the weakest performance with unimanual control. Thus, hypothesis H1 is clearly substantiated. This result was found for the path length $path_{PE}$, the RMS of the position error of the pipe end $RMS(P_{PE}^{diff})$ and the maximum absolute position error $MAX(|P_{PE}^{diff}|)$. The time t needed for task completion showed no significant effect. I.e. the test subjects used, in average, the same time for all three conditions. This suits to the instruction to focus on the steadiness of the pipe end rather than on the time of completion.

No significant effects have been found in dimension y for the position error $RMS(P_{PE}^{diff})$. This can be explained since, in contrast to x- and z-dimension, the motions in y-dimension are less affected by unintended rotations in the left pipe end (grasping point).

The test subjects achieved similar results for both bimanual approaches. Based on statistical analyzes we did not find evidence supporting hypothesis H2. This might be due to the small sample size ($N = 10$) and hence low statistical power. Additional descriptive tests (Cohen's d as the difference between the two group means divided by the pooled standard deviation for the data [35]) at least indicate small effect sizes, for RMS of the position error $RMS(P_{PE}^{diff})$, as the most meaningful criterion, when comparing both bimanual approaches. Comparing the bimanual approaches revealed a small effect size for the x-dimension ($d = 0.28$) and even a large effect size for the z-dimension ($d = 1.20$) providing initial evidence in favor of the task allocation approach.

This article has been accepted for publication in a future issue of this journal, but has not been fully edited. Content may change prior to final publication. Citation information: DOI 10.1109/TOH.2018.2809746, IEEE Transactions on Haptics

Mental and physical workload ratings indicate that despite the short training time, the test subjects got used to the novel interaction concept quickly with a moderate level of workload. The increased task performance in the bimanual approaches was not achieved at the cost of mental workload. Effect sizes (Cohen's d) showed large effects sizes for the mental ($d = 1.04$) and physical workload ($d = .80$) when comparing condition 1-3. Furthermore, a small effect size was evident for mental ($d = 0.37$) and a moderate effect size for physical workload ($d = 0.56$) when comparing condition 2-3. Obviously, the task allocation reduces users' subjective mental and physical workload.

8 Conclusion

In this paper, a multi-DoF implementation of the haptic augmentation concepts of virtual grasping point and task allocation has been introduced. These concepts have been designed as new modules of the MPMT. The virtual grasping point method was successfully extended for online adaptation of the virtual grasping point distance and improved concerning the pipe's control using opposing forces. The task allocation approach has been enhanced for higher coupling rigidity. Furthermore, a method for the reduction of negative effects due to the robot workspace constraints has been presented.

The experiments showed that the manipulation of a long object by one slave robot arm could be eased significantly by the haptic augmentation approaches. Regarding the mean deviation of desired and real pipe end positions in the experiments, the Cartesian task allocation improved the accuracy during the reorientation of the long object additionally, though the user study showed no significant improvements. The position following of the three devices, the virtual and real grasping points was satisfactory even for roundtrip delays of 40ms.

The user study revealed that the test subjects achieved significantly better task performance with bimanual compared to unimanual control. In addition, descriptive tests of the bimanual approaches showed different effect sizes in favor of the task allocation.

In future, further user studies should be performed in real world considering contacts with an environment. In the teleoperation setup, a position-force measured architecture applying force sensor information should be integrated in the master-slave coupling.

Appendix A
Cooperatively Grasping Slave Robots

The focus of this paper lies on the increase of rotational precision in a Dual-Master-Single-Slave through the virtual grasping point concept. To underline the generality and adaptability of this concept and the MPMT, a Single-Master-Dual-Slave system [36] based on the same modules is introduced here.

Often, two slave robots are applied to grasp and manipulate one object cooperatively since the load capacity, rigidity and dexterity of the system can be increased [37]. Also, in a Dual-Master-Dual-Slave setup with two separate bilateral sets of masters and slaves, the robustness to single point failure is improved and the level of safety is increased due to the distribution of kinetic energy on two robotic systems [1]. Still, the grasp quality is disturbed if the operator does not synchronously move two master devices controlling one slave robot each [38]. In contrast, if one master device controls a point on the cooperatively grasped object (compare Fig. 27), a higher robustness in the cooperative grasp can be achieved since the slave robots have a fixed kinematic coupling. As depicted in Fig. 27, the master M can control the virtual grasping point VG on the link between right slave S_R and left slave S_L. The virtual grasping point VG can be located at a distance d_1 from the center of the connecting axis D. The desired distance between the slaves is constant such that the grasping positions on the manipulated object are more robust than in a Dual-Master-Dual-Slave system in which one master controls slave S_L and another, S_R. The presented concept is similar to [39]. Here, the passivity criterion assures $\mathscr{L}_2$-stability whereas in [39], no stability proof has been accomplished.

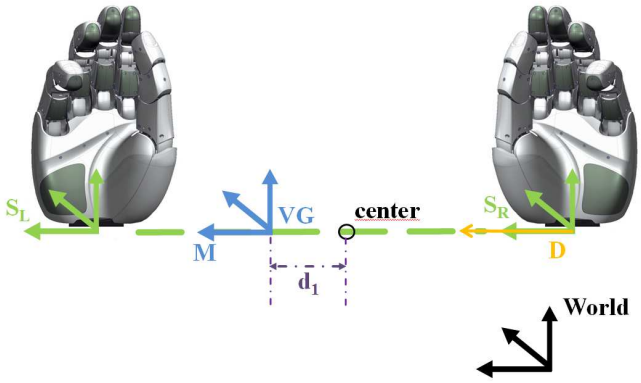

Fig. 27. Kinematically Coupled Slaves in a Single-Master-Dual-Slave System

A.1 Implementation

The virtual grasping point position VG between the left slave S_L and the right slave S_R can be calculated as follows:

$$ {}^{W}p_{VG}^{t_0} = {}^{W}p_{S_L}^{t_0} - ({}^{W}p_{S_L}^{t_0} - {}^{W}p_{S_R}^{t_0})(0.5 + d_1), \tag{53} $$

with the distance from the center d_1 (see Fig. 27). The rotation matrix ${}^{W}R_{VG}^{t_0}$ of the homogenous transform ${}^{W}H_{VG}^{t_0}$

$$ {}^{W}H_{VG}^{t_0} = \begin{bmatrix} {}^{W}R_{VG}^{t_0} & {}^{W}p_{VG}^{t_0} \\ 0 & 1 \end{bmatrix}, \tag{54} $$

can be calculated with two arbitrary vectors and one vector parallel to the connecting axis D through ${}^{W}p_{S_L}^{t_0}$ and ${}^{W}p_{S_R}^{t_0}$ (compare Fig. 27):

$$ b_1 = {}^{W}p_{S_L}^{t_0} - {}^{W}p_{S_R}^{t_0}, \tag{55} $$

$$ b_2 = \begin{bmatrix} 0 \\ -b_1(3) \\ b_2(2) \end{bmatrix}, \tag{56} $$

$$ b_3 = b_1 \times b_2 \quad \text{and} \tag{57} $$

$$ {}^{W}R_{VG}^{t_0} = [b_1/\|b_1\|_2, b_2/\|b_2\|_2, b_3/\|b_3\|_2]. \tag{58} $$

The desired pose of the grasping point ${}^{W}H_{VG}^{des}$ has to be calculated with respect to the incremental motion of the master M:

$$ {}^{W}p_{VG}^{des} = {}^{W}p_{VG}^{t_0} + {}^{W}p_{M} - {}^{W}p_{M}^{t_0}, \tag{59} $$

$$ {}^{W}R_{VG}^{des} = {}^{W}R_{M}\,{}^{M}R_{W}^{t_0}\,{}^{W}R_{VG}^{t_0}, \tag{60} $$

$$ {}^{W}H_{VG}^{des} = \begin{bmatrix} {}^{W}R_{VG}^{des} & {}^{W}p_{VG}^{des} \\ 0 & 1 \end{bmatrix}. \tag{61} $$

This article has been accepted for publication in a future issue of this journal, but has not been fully edited. Content may change prior to final publication. Citation information: DOI 10.1109/TOH.2018.2809746, IEEE Transactions on Haptics

The slave poses ${}^{W}H_{S_{L/R}}$ have to be transformed into the right coordinate frame ${}^{W}H_{\tilde{S}_{L/R}}$:

$$ {}^{W}H_{\tilde{S}_{L/R}} = \begin{bmatrix} {}^{W}R_{\tilde{S}_{L/R}} & {}^{W}p_{S_{L/R}} \\ 0 & 1 \end{bmatrix}, \text{ with} \tag{62} $$

$$ {}^{W}R_{\tilde{S}_{L/R}} = {}^{S_{L/R}}R^{t_0}_{VG_{L/R}}\, {}^{W}R_{S_{L/R}}, \tag{63} $$

where ${}^{S_{L/R}}R^{t_0}_{VG_{L/R}}$ is the rotation matrix from the respective slave to the grasping frame

$$ {}^{S_{L/R}}R^{t_0}_{VG_{L/R}} = {}^{W}R^{t_0}_{VG}\, {}^{S_{L/R}}R^{t_0}_{W}. \tag{64} $$

The desired positions of the slaves ${}^{W}H^{des}_{\hat{S}_{L/R}}$ can be calculated with the initial distance of the respective slave ${}^{W}H^{t_0}_{\tilde{S}_{L/R}}$ and desired grasping point ${}^{W}H^{des,t_0}_{VG}$ in base frame:

$$ {}^{W}H^{des}_{\hat{S}_L} = {}^{W}H^{des}_{VG}\, {}^{VG}H^{des,t_0}_{W}\, {}^{W}H^{t_0}_{\tilde{S}_L}, \tag{65} $$

$$ {}^{W}H^{des}_{\hat{S}_R} = {}^{W}H^{des}_{VG}\, {}^{VG}H^{des,t_0}_{W}\, {}^{W}H^{t_0}_{\tilde{S}_R}. \tag{66} $$

With a separate input s (e.g. a pair of buttons), the desired slave positions can be moved on axis D to perform the grasping:

$$ {}^{W}H^{des}_{S_L} = \begin{bmatrix} {}^{W}R^{des}_{\hat{S}_L} & {}^{W}p^{des}_{\hat{S}_L} + {}^{W}R^{des}_{\hat{S}_L} se \\ 0 & 1 \end{bmatrix}, \tag{67} $$

$$ {}^{W}H^{des}_{S_R} = \begin{bmatrix} {}^{W}R^{des}_{\hat{S}_R} & {}^{W}p^{des}_{\hat{S}_R} - {}^{W}R^{des}_{\hat{S}_R} se \\ 0 & 1 \end{bmatrix}, \text{ with} \tag{68} $$

$$ e = \begin{bmatrix} 1 \\ 0 \\ 0 \end{bmatrix}. \tag{69} $$

Two spatial springs are sufficient in the proposed multilateral system. Spring A couples master M with slave S_L and the second spring B couples the master M with slave S_R. The respective reference frames of the two coupling springs are listed in Table 7. As the wrench output is in the frame of ${}^{W}H_1$, the wrench has

TABLE 7
Spring Inputs

Spring	${}^{W}H_1$	${}^{W}H_2$
A	${}^{W}H_{\tilde{S}_L}$	${}^{W}H^{des}_{S_L}$
B	${}^{W}H_{\tilde{S}_R}$	${}^{W}H^{des}_{S_R}$

to be transformed into base frame in order to calculate the wrench commanded to the hardware

$$ {}^{S_L}W^A = {}^{S_L}\overline{T}_W\, {}^{W}\overline{T}_{\tilde{S}_L}\, {}^{\tilde{S}_L}W^A, \tag{70} $$

$$ {}^{M}W^A = {}^{M}\overline{T}_W\, {}^{W}\overline{T}_{\tilde{S}_L}\, \tilde{T}^{\tilde{S}_L}\tilde{W}^A, \tag{71} $$

$$ {}^{S_R}W^B = {}^{S_R}\overline{T}_W\, {}^{W}\overline{T}_{\tilde{S}_R}\, {}^{\tilde{S}_R}W^B, \tag{72} $$

$$ {}^{M}W^B = {}^{M}\overline{T}_W\, {}^{W}\overline{T}_{\tilde{S}_R}\, \tilde{T}^{\tilde{S}_R}\tilde{W}^B, \tag{73} $$

with $\tilde{W}^i = -W^i$ and

$$ \tilde{T} = \left[\begin{array}{ccc|c} & \mathbf{I}_3 & & \mathbf{0}_3 \\ 0 & 0 & 0 & \\ 0 & 0 & 0.5 \pm (d_1 + s) & \mathbf{I}_3 \\ 0 & 0.5 \pm (d_1 + s) & 0 & \end{array}\right]. \tag{74} $$

A.2 Passivity

As depicted in Fig. 28, the network representation of the multilateral system for cooperative slaves is based on the formerly introduced passive modules. Analogous to the input a in Section 3, the input s does not violate the passivity condition.

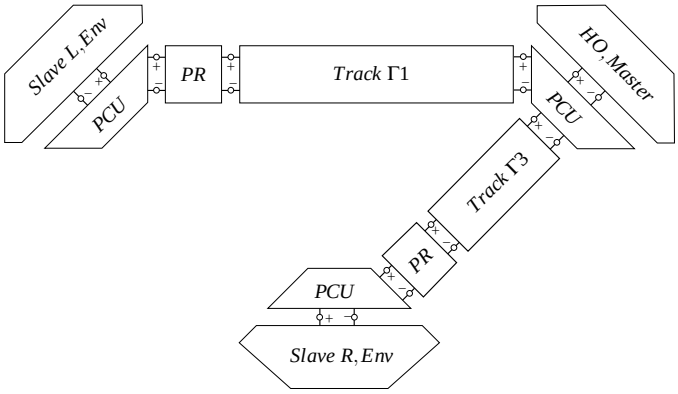

Fig. 28. Single-Master-Multi-Slave System for Cooperative Slave Grasping

Two additional PI controllers or tracks respectively can be added to stiffen the control loop as depicted in Fig. 29. Then, the master is coupled to each device by one spring in the master position and a second spring in the position of the respective slave. Through the passive design of the track modules, the passivity criterion is fulfilled.

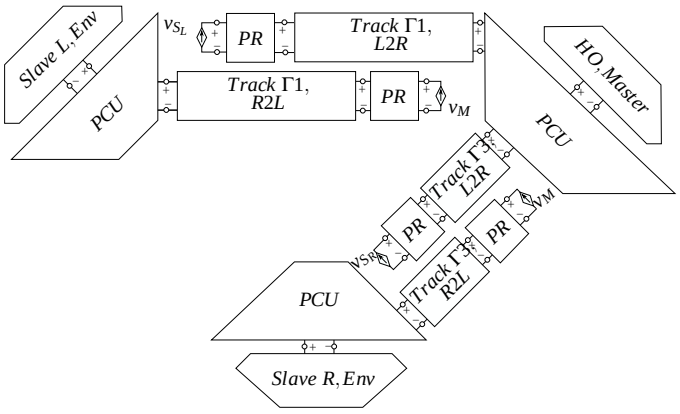

Fig. 29. Single-Master-Multi-Slave System for Cooperative Slave Grasping with Additional Spatial Springs

A.3 Experiments

The following experiment was performed with an Omega.7 [40] master input device and the DLR HUG. The coupling was implemented with four spatial springs according to Fig. 29.

In Exp. 30, a rotation around the x-axis and a translational motion on the x-axis were commanded by the master device. Plot Exp. 30a depicts the position tracking of the right slave robot ${}^{W}H_{S_R}$ and the desired slave robot pose ${}^{W}H^{des}_{S_R}$. α, β and γ describe the rotations around x, y and z axis respectively. The commanded rotation around the x-axis is well tracked by the slave device. The translational position accuracy is lower which might result from workspace related disturbances. Fig. 30b presents the 3D motion of the multilateral system. The kinematic coupling via four spatial springs provides the desired performance.

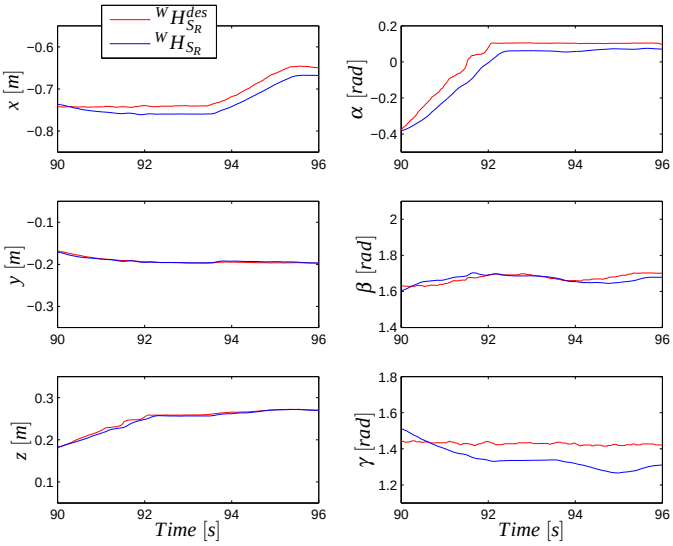

(a) Position Tracking

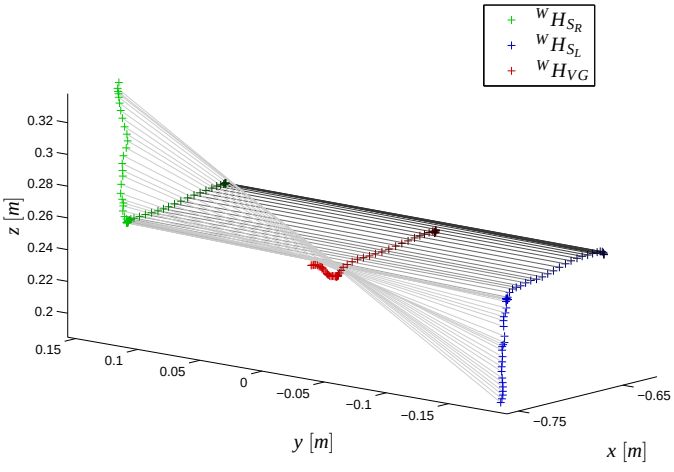

(b) 3D Motion

Fig. 30. Kinematically Coupled Slave Robots in a Multilateral Setup (Devices M, S_R, S_L and Tracks Γ1 $L2R$, Γ1 $R2L$, Γ2 $L2R$, Γ2 $R2L$)

REFERENCES

[1] D. Lee and M. W. Spong, "Bilateral teleoperation of multiple cooperative robots over delayed communication networks: theory," in *International Conference on Robotics and Automation*. IEEE, 2005, pp. 360–365.

[2] R. Mohajerpoor, I. Sharifi, H. A. Talebi, and S. M. Rezaei, "Adaptive bilateral teleoperation of an unknown object handled by multiple robots under unknown communication delay," *IEEE International Conference on Advanced Intelligent Mechatronics*, pp. 1158 – 1163, 2013.

[3] S. Nudehi, R. Mukherjee, and M. Ghodoussi, "A shared-control approach to haptic interface design for minimally invasive telesurgical training," *Control Systems Technology, IEEE Transactions on*, vol. 13, no. 4, pp. 588–592, 2005.

[4] M. Shahbazi, S. F. Atashzar, H. A. Talebi, and R. V. Patel, "An expertise-oriented training framework for robotics-assisted surgery," in *Robotics and Automation (ICRA), 2014 IEEE International Conference on*. IEEE, 2014, pp. 5902–5907.

[5] E. Nuno, R. Ortega, L. Basanez, and D. Hill, "Synchronization of networks of nonidentical euler-lagrange systems with uncertain parameters and communication delays," *Transactions on Automatic Control*, vol. 56, pp. 935–941, 2011.

[6] T. Kanno and Y. Yokokohji, "Multilateral teleoperation control over time-delayed computer networks using wave variables," *Haptics Symposium*, pp. 125–131, 2012.

[7] M. Panzirsch, J. Artigas, J.-H. Ryu, and M. Ferre, "Multilateral control for delayed teleoperation," *IEEE International Conference on Advanced Robotics*, pp. 1–6, 2013.

[8] M. Panzirsch, R. Balachandran, and J. Artigas, "Cartesian task allocation for cooperative, multilateral teleoperation under time delay," in *Robotics and Automation (ICRA), 2015 IEEE International Conference on*. IEEE, 2015, pp. 312–317.

[9] M. Panzirsch, R. Balachandran, J. Artigas, C. Riecke, M. Ferre, and A. Albu-Schäffer, "Haptic intention augmentation for cooperative teleoperation," in *IEEE International Conference on Robotics and Automation*, 2017.

[10] P. Malysz and S. Sirouspour, "Trilateral teleoperation control of kinematically redundant robotic manipulators," *The International Journal of Robotics Research*, vol. 30, pp. 1643–1664, 2011.

[11] P. Malysz and S. Sirouspour, "Cooperative teleoperation control with projective force mappings," *IEEE Haptics Symposium*, pp. 301 – 308, 2010.

[12] S. Katsura, T. Suzuyama, and K. Ohnishi, "A realization of multilateral force feedback control for cooperative motion," *IEEE Transactions on Industrial Electronics*, vol. 54, pp. 3298 – 3306, 2007.

[13] D. G. Lee, G. R. Cho, M. S. Lee, B.-S. Kom, S. Oh, and H. I. Son, "Human-centered evaluation of multi-user teleoperation for mobile manipulator in unmanned offshore plants," *IEEE International Conference on Intelligent Robots And Systems*, pp. 5431–5438, 2013.

[14] P. Malysz and S. Sirouspour, "A kinematic control framework for single-slave asymmetric teleoperation systems," *IEEE Transactions on Robotics*, vol. 27, pp. 901 – 917, 2011.

[15] P. Malysz and S. Sirouspour, "Task performance evaluation of asymmetric semiautonomous teleoperation of mobile twin-arm robotic manipulators," *IEEE Transactions on Haptics*, vol. 6, pp. 484 – 495, 2013.

[16] O. Mohareri, C. Schneider, and S. Salcudean, "Bimanual telerobotic surgery with asymmetric force feedback: a davinci® surgical system implementation," in *Intelligent Robots and Systems (IROS 2014), 2014 IEEE/RSJ International Conference on*. IEEE, 2014, pp. 4272–4277.

[17] J. A. Esclusa, J. V. i Buxó, C. Preusche, and G. Hirzinger, "Time Domain Passivity - based Telepresence with Time Delay," in *IEEE International Conference on Intelligent Robots And Systems (IROS)*, 2006.

[18] N. Chopra, M. W. Spong, and R. Lozano, "Synchronization of bilateral teleoperators with time delay," *Automatica*, vol. 44, no. 8, pp. 2142–2148, 2008.

[19] M. Franken, S. Stramigioli, S. Misra, C. Secchi, and A. Macchelli, "Bilateral telemanipulation with time delays: A two-layer approach combining passivity and transparency," *Robotics, IEEE Transactions on*, vol. 27, no. 4, pp. 741–756, 2011.

[20] J. C. Willems, "Dissipative dynamical systems part i: General theory," *Archive for rational mechanics and analysis*, vol. 45, no. 5, pp. 321–351, 1972.

[21] A. J. Van Der Schaft and A. Van Der Schaft, *L2-gain and passivity techniques in nonlinear control*. Springer, 2000, vol. 2.

[22] J. Artigas, J.-H. Ryu, C. Preusche, and G. Hirzinger, "Network representation and passivity of delayed teleoperation systems," in *Intelligent Robots and Systems (IROS), 2011 IEEE/RSJ International Conference on*. IEEE, 2011, pp. 177–183.

[23] J. Artigas, J.-H. Ryu, and C. Preusche, "Time domain passivity control for position-position teleoperation architectures," *Presence: Teleoperators and Virtual Environments*, vol. 19, no. 5, pp. 482–497, 2010.

[24] J. L. Wyatt Jr, L. O. Chua, J. W. Gannett, I. C. Goknar, and D. N. Green, "Energy concepts in the state-space theory of nonlinear n-ports: Part i-passivity," *Circuits and Systems, IEEE Transactions on*, vol. 28, no. 1, pp. 48–61, 1981.

[25] M. Panzirsch, J. Artigas, A. Tobergte, P. Kotyczka, C. Preusche, A. Albu-Schaeffer, and G. Hirzinger, "A peer-to-peer trilateral passivity control for delayed collaborative teleoperation," *EuroHaptics*, vol. 12, pp. 395–406, 2012.

[26] H. V. Quang and J.-H. Ryu, "Stable multilateral teleoperation with time domain passivity approach," *IEEE International Conference on Intelligent Robots And Systems*, pp. 5890 – 5895, 2013.

[27] H. LeBlanc, E. Eyisi, N. Kottenstette, X. Koutsoukos, and J. Sztipanovits, "A passivity-based approach to deployment in multi-agent networks," in *Informatics in Control, Automation and Robotics*. Springer Berlin Heidelberg, 2011, pp. 135–149.

[28] N. Y. Chong, T. Kotoku, K. Ohba, and K. Komoriya, "Remote coordinated controls in multiple telerobot cooperation," *IEEE International Conference on Robotics And Automation*, pp. 3138 – 3143, 2000.

[29] A. Ghorbanian, S. Rezaei, A. Khoogar, M. Zareinejad, and K. Baghestan, "A novel control framework for nonlinear time-delayed dual-master/single-slave teleoperation," *ISA transactions*, vol. 52, no. 2, pp. 268–277, 2013.

[30] J.-H. Ryu, J. Artigas, and C. Preusche, "A passive bilateral control scheme for a teleoperator with time-varying communication delay," *Elsevier Journal of Mechatronics*, vol. 20, pp. 812–823, October 2010.
[31] R. Balachandran, J. Artigas, U. Mehmood, and J.-H. Ryu, "Performance comparison of wave variable transformation and time domain passivity approaches for time-delayed teleoperation: Preliminary results," in *Intelligent Robots and Systems (IROS), 2016 IEEE/RSJ International Conference on*. IEEE, 2016, pp. 410–417.
[32] J. Behr, U. Bockholt, and D. Fellner, "Instantrealitya framework for industrial augmented and virtual reality applications," in *Virtual Reality & Augmented Reality in Industry*. Springer, 2011, pp. 91–99.
[33] B. G. Witmer and M. J. Singer, "Measuring presence in virtual environments: A presence questionnaire," *Presence: Teleoperators and virtual environments*, vol. 7, no. 3, pp. 225–240, 1998.
[34] R. S. Kennedy, N. E. Lane, K. S. Berbaum, and M. G. Lilienthal, "Simulator sickness questionnaire: An enhanced method for quantifying simulator sickness," *The international journal of aviation psychology*, vol. 3, no. 3, pp. 203–220, 1993.
[35] J. Cohen, "Statistical power analysis for the behavioral sciences . hilsdale," *NJ: Lawrence Earlbaum Associates*, vol. 2, 1988.
[36] A. Kheddar, C. Tzafestas, P. Coiffet, T. Kotoku, S. Kawabata, K. Iwamoto, K. Tanie, I. Mazon, C. Laugier, and R. Chellali, "Parallel multi-robots long distance teleoperation," in *International Conference on Advanced Robotics*. IEEE, 1997, pp. 1007–1012.
[37] K. Kosuge, J. Ishikawa, K. Furuta, and M. Sakai, "Control of single-master multi-slave manipulator system using vim," in *Robotics and Automation, 1990. Proceedings., 1990 IEEE International Conference on*. IEEE, 1990, pp. 1172–1177.
[38] D. Lee, O. Martinez-Palafox, and M. W. Spong, "Bilateral teleoperation of multiple cooperative robots over delayed communication networks: Application," in *International Conference on Robotics and Automation*. IEEE, 2005, pp. 366–371.
[39] G. Hwang, P. T. Szemes, N. Ando, and H. Hashimoto, "Development of a single-master multi-slave tele-micromanipulation system," *Advanced Robotics*, vol. 21, no. 3-4, pp. 329–349, 2007.
[40] F. Dimension, "Omega.7 overview," *URL http://www.forcedimension.com/products/omega-7/overview*, 2017.

Michael Panzirsch was born in Donauwörth, Germany, in 1985. He received his Diploma in mechanical engineering from the Technical University of Munich (TUM) in 2010. Since then he is a researcher at the Department for Analysis and Control of Advanced Robotic Systems of the german aerospace center (DLR) in Oberpfaffenhofen. Currently he is writing his doctoral thesis on multilateral teleoperation. His main areas of research interests are teleoperation of static and mobile robots and haptics.

Ribin Balachandran received a bachelor degree in Electrical and Electronics Engineering from National Institute of Technology, Surathkal-India in 2009 and a master degree in Automation and Robotics from Techincal University of Dortmund, Germany in 2013. He is a researcher at the German Aerospace Center (DLR) in the Institute of Robotics and Mechatronics (Oberfpaffenhofen, Germany) since 2013. His main research areas are time-delayed teleoperation, haptics and control for robotics.

Bernhard Weber Bernhard Weber received his PhD degree from the University of Wuerzburg, Germany, in 2008. He is with the DLR since 2008, first at the Human Factors Department of the Institute of Flight Guidance, in Brunswick and since 2010 as human factors expert at the Institute of Robotics and Mechatronics. His main research interests are human-robot-interaction and evaluation of human-machine-interfaces for surgical, space robotic and virtual reality applications.

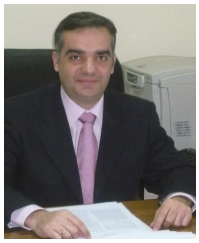

Manuel Ferre Laurea Degree in Control Engineering and Electronics in 1992 and PhD in Automation and Robotics in 1997, at the Universidad Politcnica de Madrid (UPM). In 1990, he started his research activity at this university, where he is currently a Profesor Titular since 2000. In 1997, he worked as a PostDoc in the Human-Machine System Laboratory of Massachusetts Institute of Technology (MIT). He has participated and coordinated several research projects in robotics and automatic control, both at national and international programs. His research interest is focused on automatic control, advanced telerobotics, and haptics. He has three patents of haptic devices and stereoscopic video cameras. He is authos of more than 100 publications and editor of the 'Springer Series on Touch and Haptics System'. He is member of IEEE and serves as chair of the RAS Technical Committee on Telerobotics. He is also member of EuroHaptics Society where he serves as Treasurer. He has participated in International Program Committees of several conferences highlighting some editions of IROS and EuroHaptics. He was the chairman of the First Int. Workshop on Telerobotics in 2004 and hosted the EuroHaptics 2008 conference.

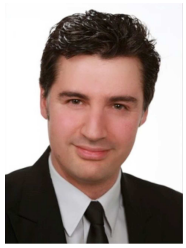

Jordi Artigas Jordi Artigas received his M.S. in electrical engineering from the Ramon Llull University (Barcelona) in 2003 and received his Ph.D. in automation and robotics from the Technical University of Madrid (UPM) in 2014. He was a visiting researcher at the PERCRO Laboratory in Scuola Santa Anna (Pisa, Italy) in 2008 and at the Korean University of Technology and Education (Seoul, Korea) in 2009 and 2012. Currently he is leading the Telemanipulation robotic systems group in the German Aerospace Center (DLR) at the Institute of Robotics and Mechatronics. He is chair of the IEEE Telerobotics Technical Committee since 2012. His main research interests include bilateral control methods for complex telemanipulation systems through delay affected communication infrastructures, physical human-robot interaction, space tele-robotics, haptics and telepresence.